

Gauge fields in graphene

M. A. H. Vozmediano,¹ M. I. Katsnelson,² and F. Guinea³

¹*Instituto de Ciencia de Materiales de Madrid,
CSIC, Cantoblanco, E-28049 Madrid, Spain.*

²*Radboud University Nijmegen,*

Institute for Molecules and Materials, Heijendaalseweg 135, 6525 AJ, Nijmegen, The Netherlands

³*Instituto de Ciencia de Materiales de Madrid, CSIC, Cantoblanco, E-28049 Madrid, Spain.*

(Dated: November 26, 2024)

The physics of graphene is acting as a bridge between quantum field theory and condensed matter physics due to the special quality of the graphene quasiparticles behaving as massless two dimensional Dirac fermions. Moreover, the particular structure of the 2D crystal lattice sets the arena to study and unify concepts from elasticity, topology and cosmology. In this paper we analyze these connections combining a pedagogical, intuitive approach with a more rigorous formalism when required.

PACS numbers:

Contents

I. Introduction	2
II. The honeycomb lattice: Spinors and geometry in two dimensions	3
A. The low energy electronic excitations of graphene. Continuum model	3
B. Topological stability of the Fermi points	4
C. Gauge fields in physics and geometry	5
D. Types of gauge fields	7
III. Topological defects in graphene	7
A. Topological defects. Formation and naturalness	8
B. The gauge approach to disclinations	9
1. Two gauge fields for a single disclination	10
2. Generalization to several defects: gauge fields arising from the holonomy	11
C. Modelling curvature. Dirac fermions in curved space	12
D. The electronic spectrum of fullerenes	14
E. Dislocations and torsion: a general relativity approach	15
IV. Strain fields	16
A. Modulations of the tight binding parameters	16
B. Gauge fields as function of the in plane strains	17
C. Out of plane displacements	18
D. Thermal fluctuations and intrinsic ripples in graphene	20
V. Observable consequences of the gauge fields: microscopic effects	24
A. Index theorems and zero energy states	24
B. Inhomogeneities in the electronic density	26
C. Strains, gauge fields, and weak (anti)localization	26
D. Modelling disorder in graphene with random gauge fields	28
E. Scattering of charge carriers by gauge fields	29
VI. Observable consequences of the gauge fields: mesoscopic effects, strains in suspended samples	32
A. Aharonov-Bohm phases in suspended samples	32
1. Electronic transport in ballistic samples	33
B. Interferences between strains and real magnetic fields	33
C. Generation of effective magnetic fields. Strain engineering	35
D. Effective electric fields	35

VII. Conclusions	36
VIII. Acknowledgments	36
A. The Dirac equation in curved space	37
B. In plane strains and effective fields in radial coordinates	39
References	40

I. INTRODUCTION

One of the sad consequences of the very fast development of physics during the last half of a century is that it has started to lose its unity. Especially, the gap between condensed matter physics which is a key ingredient of our scientific understanding a “world around us” and microphysics investigating the most fundamental laws of nature (high-energy physics, quantum field theory, gravity and cosmology, etc.) has become wider. That is why examples of fruitful exchange of ideas and methods between these two branches of physics are very important now. A prototype example of the relevance of macrophysics for microphysics is the idea of spontaneously broken symmetry which first appeared in Landau’s theory of second-order phase transitions [1] and then turned out to be one of the most important concepts in both condensed matter [2] and fundamental physics [3, 4]. Conversely, the idea of the renormalization group, being developed first to study the problem of infinities in quantum electrodynamics (QED) has been of crucial importance to solve problems of condensed matter physics as difficult as critical behavior and the Kondo problem [5–9]. The use of Mössbauer effect to check the general relativity theory [10] gives an amazing example of an entanglement of condensed matter physics, nuclear physics, and gravity.

One of the fields where condensed matter physics meets quantum field theory and cosmology is that of the superfluidity of helium 3 [11]. A recent development in material science provides a new and unexpected bridge between condensed matter and high-energy physics. The experimental discovery of graphene, a two-dimensional allotrope of carbon formed by a single carbon atom sheet, was made in 2004 when a technique called micromechanical cleavage was employed to obtain the first graphene crystals [12, 13]. The observation of a peculiar “Dirac-like” spectrum of charge carriers and an anomalous quantum Hall effect in graphene [14, 15] has ignited an enormously growing interest to this field (for a review, see [16–20]). One of the most interesting aspects of the graphene physics from a theoretical point of view is the deep and fruitful relation that it has with QED and other quantum field theory ideas [21–29]. Probably the most clear example is the Klein paradox [30, 31], a property of relativistic quantum particles of being able to penetrate with a probability of the order of unity through very high and broad potential barriers. Previously it was discussed only for experimentally unattainable (or very hard to reach) situations such as particle-antiparticle pair creation at the black hole evaporation, or vacuum breakdown at collisions of super-heavy nuclei (a rather complete reference list can be found in [32]). At the same time, it appeared to be relevant for graphene-based electronics and for electronic transport in graphene [25, 28, 33–35].

Here we focus on a particular aspect of the physics of graphene that establishes its connection with QED, field theory and gravity, namely, the appearance of gauge fields in graphene and their effect on its properties. The concept of a gauge field in general has been extensively discussed in condensed matter physics, especially, in relation with modeling different types of topological defects, phase transitions, and properties of glasses [36–40]. In the modern context of graphene the gauge fields were first introduced in [41, 42] in relation with the problem of weak localization. It is well-established by now, both experimentally and theoretically [41, 43–47], that graphene is always corrugated and covered by ripples which can be either intrinsic [38, 43, 44, 47] or induced by a roughness of substrate [45, 46]. In general, the departure from flatness of graphene leads to the appearance of an inhomogeneous pseudomagnetic gauge field [41, 42] acting on the charge carriers. This has important consequences affecting the character of quantum Hall effect in graphene, it produces an effective source of charge carrier scattering, and it can provide a mechanism for an observed charge inhomogeneity, as discussed in detail below. Whereas a smooth deformation of the graphene sheets produces a gauge field similar to the electromagnetic one, different topological defects in graphene inducing intervalley (Umklapp) processes can be considered sources of a non-Abelian gauge field [48, 49]. On the other hand the description of some topological defects as cosmic strings [50] creates an interesting connection with general relativity. This will be also described in the present review.

The work is organized as follows. Section II presents the electronic features of the model that are most relevant for the physics discussed. Section IIA gives a short description of the way in which the Dirac equation approximates the electronic states of graphene in the long wavelength limit emphasizing the need for two component wavefunctions. In subsection IIB we show the topological stability of the Fermi points in the honeycomb lattice towards small perturbations like lattice deformations or disorder. Then, in subsections IIC and IID we describe the way in which

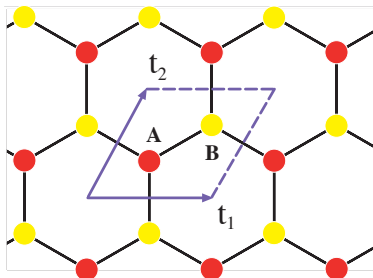


FIG. 1: (Color online) Lattice and unit cell for monolayer graphene in real space.

gauge fields were defined in physics and in geometry and we show the different types of effective gauge fields that appear in graphene associated to various disorder types. Different physical mechanisms which can contribute to these gauge fields are discussed next, in sections III (topological defects) and IV (smooth deformations). Observable effects related to the gauge fields are described in sections V (microscale gauge fields) and VI (macroscale gauge fields). Section VII presents a summary of the work, open questions, and some possible future developments. Technical aspects related to general features of spinors in a curved two dimensional surface are explained in Appendix A and some auxiliary material from the elasticity theory is presented in Appendix B.

II. THE HONEYCOMB LATTICE: SPINORS AND GEOMETRY IN TWO DIMENSIONS

A. The low energy electronic excitations of graphene. Continuum model

Monolayer graphite - graphene - consists of a planar honeycomb lattice of carbon atoms shown in Fig. 1. In the graphene structure the in-plane σ bonds are formed from $2s$, $2p_x$ and $2p_y$ orbitals hybridized in a sp^2 configuration, while the $2p_z$ orbital, perpendicular to the layer, builds up covalent bonds, similar to the ones in the benzene molecule. The σ bonds give rigidity to the structure, while the π bonds give rise to the valence and conduction bands. The electronic properties around the Fermi energy of a graphene sheet can be described by a tight binding model with only one orbital per atom, the so-called π -electron approximation because there is no significant mixing between states belonging to σ and π bands in 2D graphite. Within this approximation a basis set is provided by the Bloch functions made up of the $2p_z$ orbitals from the two inequivalent carbon atoms A and B which form the unit cell of the honeycomb lattice. One may define two Bloch wave functions to be used in a variational (tight-binding) computation of the spectrum

$$\Phi_i(\vec{K}) = \sum_{\vec{t}} e^{i\vec{K}\cdot(\vec{r}_i+\vec{t})} \Phi(\vec{r} - \vec{r}_i - \vec{t}) \quad , \quad i = A, B \quad (1)$$

where the sum runs over all the points in the direct lattice, i.e., $\vec{t} = n_1\vec{t}_1 + n_2\vec{t}_2$, (\vec{r}_A, \vec{r}_B) are the positions of the atoms in the unit cell, and $\Phi(\vec{r})$ is a real (π -type) atomic orbital. As it is well known, a simple tight-binding computation [51, 52] yields at the neutrality point a Fermi surface made of the six single points located at the corners of the hexagonal Brillouin zone. Only two of them are inequivalent and can be chosen to be located at $\vec{K}_1 = -2\vec{g}_1/3 - \vec{g}_2/3$ and $\vec{K}_2 = -\vec{K}_1$, where $\vec{t}_i \cdot \vec{g}_j = 2\pi\delta_{ij}$. A low energy expansion around any of the two Fermi points $K_{+,-}$ gives an effective hamiltonian linear in momentum which reduces to the massless Dirac equation in two dimensions derived from the Hamiltonian:

$$\mathcal{H}_0 = -\hbar v_F \int d^2\mathbf{r} \bar{\Psi}(\mathbf{r}) (i\sigma_x \partial_x + i\sigma_y \partial_y) \Psi(\mathbf{r}) \quad , \quad (2)$$

where σ_i are the Pauli matrices, $v_F = (3ta)/2$, t is the nearest-neighbor hopping parameter, and $a = 1.42 \text{ \AA}$ is the distance between nearest carbon atoms.

The components of the two-dimensional spinor:

$$\Psi(\vec{r}) = \begin{pmatrix} \Psi_1(\mathbf{r}) \\ \Psi_2(\mathbf{r}) \end{pmatrix} \quad (3)$$

correspond to the amplitude of the wavefunction in each of the two sublattices which build up the honeycomb structure. The two Fermi points of the honeycomb lattice give rise to two similar equations related by time reversal symmetry.

We can combine the two spinors attached to each Fermi point into a four component Dirac spinor and write the four-dimensional Hamiltonian:

$$H_D = -iv_F \hbar (1 \otimes \sigma_1 \partial_x + \tau_3 \otimes \sigma_2 \partial_y), \quad (4)$$

where σ and τ matrices are Pauli matrices acting on the sublattice and valley degree of freedom respectively.

Summarizing, the internal degrees of freedom of charge carriers in graphene are: Sublattice index (pseudospin), valley index (flavor) and real spin, each taking two values. The real spin is irrelevant for the issues discussed in this review and will not be taken into account except for an additional degeneracy factor 2 in some quantities.

B. Topological stability of the Fermi points

The properties of graphene presented in this work as well as most of the exotic properties of the material lie on the special character of its low energy excitations obeying a massless two dimensional Dirac equation. Hence it is important to establish the robustness of the low energy description under small lattice deformations, disorder and other possible low energy perturbations. In this section we will analyze the existence and stability of the Fermi points in the graphene lattice. A related issue is the possibility to open and control a gap in the material, crucial for electronic applications. We will analyze under which conditions a gap can open in neutral graphene. We will see that the Dirac points in graphene are topologically preserved under rather general circumstances and Coulomb interactions, stress, phonons, and other moderate perturbations of the lattice will not open a gap. The analysis of this section follows closely ref. [53].

The discrete symmetries of the system playing a very important role in the analysis we will summarize them first. As it was described in Section II A, the Fermi surface of neutral graphene consists of two independent Fermi points that can be chosen in the Brillouin zone to be located at K and $-K$. The effective low energy Hamiltonians around these points are

$$H(\vec{K}_1 + \vec{k}) \sim \begin{pmatrix} 0 & k^* \\ k & 0 \end{pmatrix} = k_x \sigma_x + k_y \sigma_y, \quad (5)$$

and

$$H(-\vec{K}_1 + \vec{k}) \sim \begin{pmatrix} 0 & -k \\ -k^* & 0 \end{pmatrix} \sim -k_x \sigma_x + k_y \sigma_y. \quad (6)$$

where $k \equiv k_x + ik_y$ and σ_i are the Pauli matrices.

A gap will be opened by a k -independent, translationally invariant perturbation of the type

$$H(\vec{K}_1 + \vec{k}) \rightarrow \begin{pmatrix} a_z & k^* + a^* \\ k + a & -a_z \end{pmatrix} \quad (7)$$

where $a \equiv a_x + ia_y$. The spectrum becomes $E = \pm \sqrt{a_z^2 + |k + a|^2}$ and a gap $2|a_z|$ is generated. However as we will see, such a perturbation is not allowed if the discrete symmetries of the system are to be respected. The two relevant discrete symmetries in graphene are time-reversal $T : t \rightarrow -t$ and spatial inversion $I : (x, y) \rightarrow (-x, -y)$. The reality of the π orbitals implies that time reversal merely reverses \vec{K}

$$T\Phi_i(\vec{K}) = \Phi_i^*(\vec{K}) = \Phi_i(-\vec{K}) \quad (8)$$

whereas the spatial inversion also exchanges the two types of atoms

$$I\Phi_A(\vec{K}) = \Phi_B(-\vec{K}) \quad , \quad I\Phi_B(\vec{K}) = \Phi_A(-\vec{K}). \quad (9)$$

Invariance under these symmetries imposes the following constraints on the Hamiltonians:

$$\begin{aligned} T : H(\vec{K}) &= H^*(-\vec{K}) \\ I : H(\vec{K}) &= \sigma_x H(-\vec{K}) \sigma_x. \end{aligned} \quad (10)$$

From eqs. (9) and (10) we see that none of the two symmetries are obeyed for the effective description around a single Fermi point. The graphene system is only invariant under T and I individually if both Fermi points are considered simultaneously. Nevertheless the product TI imposes a constraint on the form of $H(\vec{K})$ at each given Fermi point:

$$TI : H(\vec{K}) = \sigma_x H^*(\vec{K}) \sigma_x. \quad (11)$$

If the allowed perturbation respects TI this implies that $H_{11}(\vec{K}) = H_{22}(\vec{K})$, what enforces $a_z = 0$ in (7) and no gap opens.

This has an interesting topological interpretation, which extends the previous arguments to k -dependent —but translationally invariant— perturbations. The low energy hamiltonian $H(\vec{K}_1 + \vec{k})$ in (5) defines a map from the circle $k_x^2 + k_y^2 = R^2$ to the space of 2×2 Hamiltonians $H = \vec{h} \cdot \vec{\sigma}$:

$$k = R e^{i\theta} \rightarrow (h_x, h_y, h_z) = R(\cos \theta, \sin \theta, 0). \quad (12)$$

Since Fermi points correspond to zeroes of the determinant $-Det(H) = h_x^2 + h_y^2 + h_z^2$, a perturbation will be able to create a gap only if the loop represented by the map (12) is contractible in the space of Hamiltonians with non-vanishing determinants, which is just $R^3 - \{0\}$. This is clearly the case, since $\pi_1(R^3 - \{0\}) = \pi_1(S^2) = 0$. On the other hand, Hamiltonians invariant under TI are represented by points in R^2 , and we have

$$\pi_1(R^2 - \{0\}) = \pi_1(S^1) = Z \quad (13)$$

This means that non-trivial maps such as the ones implied by (5) can only be extended to the interior of the circle by going through the origin, i.e., by having at least one zero. This precludes the creation of a gap. The non-trivial topological charge associated to the topological stability of each individual Fermi point in graphene is simply the winding number which can be computed from

$$N = \frac{1}{4\pi i} \int_0^{2\pi} d\theta \text{Tr}(\sigma_z H^{-1} \partial_\theta H). \quad (14)$$

It is important to realize that the two Fermi points have opposite winding numbers implying that they could annihilate mutually if brought together by a perturbation.

The nontrivial topological charge associated to the topological stability of individual Fermi point in very general 2D systems has been discussed in [54] and in [55–57] in the context of topological insulators.

C. Gauge fields in physics and geometry

Gauge invariance plays a key role in the quantum field theory (QFT) description of fundamental forces between elementary particles. The seemingly abstract concept of a non-Abelian gauge field introduced first in QFT to describe the electroweak interaction followed by the experimental discovery of the W and Z bosons is one of the most impressive achievements of theoretical physics. Before introducing the various gauge fields appearing associated to the physics of graphene and in order to clarify their specific nature we will make a brief description of the classical concept of gauge invariance and of the associated gauge fields.

The concept of gauge invariance emerged from classical electrodynamics. In particular the electromagnetic field (\mathbf{E}, \mathbf{B}) is expressed in terms of potentials (Φ, \mathbf{A}) through:

$$\mathbf{E} = -(\nabla\Phi + \partial_t\mathbf{A}) \ , \ \mathbf{B} = \nabla \wedge \mathbf{A}. \quad (15)$$

The fields do not change under the transformation

$$\mathbf{A} \rightarrow \mathbf{A} + \nabla\chi \ , \ \Phi \rightarrow \Phi - \partial_t\chi, \quad (16)$$

where χ is an arbitrary (smooth) function of space. This invariance was shown to survive to the Quantum Mechanics description of a charged spinless particle in an electromagnetic field provided that the wave function was simultaneously transformed to

$$\Psi \rightarrow \Psi \exp(ie\chi). \quad (17)$$

The relativistic wave equation for a spinless particle with charge e interacting with electromagnetic fields is derived by first performing the substitution $p^\mu \rightarrow p^\mu - eA^\mu$, where $A^\mu = (A^0 = \Phi, \mathbf{A})$ is the 4-vector electromagnetic potential

and then performing the usual substitution $p_\mu \rightarrow i\hbar\partial_\mu$. A formal solution for the wave function of a particle interacting with the electromagnetic potential A^μ can be written in terms of the solution without interaction Ψ_0 as

$$\Psi = \exp \left[-ie \int A^\mu dx_\mu \right] \Psi_0. \quad (18)$$

The original discovery by V. Fock was that the quantum dynamics, i. e. the form of the quantum equation, remains unchanged by the transformations (16) if the wave function of the particle is multiplied by a local (space-time-dependent) phase. The modern description and the term “gauge invariance” was established by H. Weyl. An interesting account of the historical development of the gauge concept is given in [58].

The first example of a QFT gauge model is four dimensional QED. A free spin 1/2 Dirac fermion with charge e and mass m is described by the action

$$S_\Psi = \int d^4x \bar{\Psi} [\gamma^\mu \partial_\mu + m] \Psi, \quad (19)$$

which is invariant under the global $U(1)$ group transformations:

$$\Psi(x) \rightarrow U\Psi(x), \quad \bar{\Psi}(x) \rightarrow U^*\bar{\Psi}(x), \quad U = \exp(ie\chi), \quad (20)$$

where χ is a constant. Gauge invariance requires invariance of the action under the *local* group of transformations obtained by replacing $\chi \rightarrow \chi(x)$. This can be achieved by replacing the derivative in (19) by the covariant derivative $D_\mu = \partial_\mu + ieA_\mu$: Under a local $U(1)$ transformation defined by (20) with a space-time dependent function $\chi(x)$, $A_\mu(x)$ transforms as $A_\mu \rightarrow A_\mu - \partial_\mu\chi$, a generalization of (16).

The invariance of the Maxwell equations under special relativity allows a formulation of (classical) electromagnetism in terms of quadrivectors and tensors. The equations can be written in a covariant way by introducing the electromagnetic tensor $F_{\mu\nu}$ defined by

$$F_{0i} = E_i, \quad F_{ij} = -\epsilon_{ijk}B_k, \quad (21)$$

and the quadricurrent $J^\mu = (\rho, \mathbf{J})$ made of the charge density and the current. In terms of these geometric objects the four Maxwell equations reduce to

$$\partial_\lambda F_{\mu\nu} + \partial_\mu F_{\nu\lambda} + \partial_\nu F_{\lambda\mu} = 0, \quad (22)$$

$$\partial_\mu F^{\mu\nu} = J^\nu. \quad (23)$$

The conservation of the current $\partial_\nu J^\nu = 0$ follows from the antisymmetry of $F_{\mu\nu}$. The first equation is identified as a Bianchi identity that can be integrated by introducing a gauge field A_μ such that $F_{\mu\nu} = \partial_\mu A_\nu - \partial_\nu A_\mu$. It is readily verified that two gauge fields related by the gauge transformation $A'_\mu = A_\mu - \partial_\mu\Omega$ give rise to the same electromagnetic tensor field. Maxwell's equations can be derived from the action

$$S(A, J) = \int d^4x [F_{\mu\nu}F^{\mu\nu} + J_\mu A^\mu], \quad (24)$$

which is precisely the full QED action.

The concepts of gauge fields and covariant derivatives can be translated into the language of differential geometry, based on differential forms. In general, the gauge field has a mathematical interpretation as a Lie-valued connection and is used to construct covariant derivatives acting on fields, whose form depends on the representation of the group under which the field transforms (for global transformations). The field tensor $F_{\mu\nu}$ is a curvature 2-form given by the commutator of two covariant derivatives. It is an element of the Lie algebra associated to the gauge group. The gauge connection generates parallel transport of the geometric objects under gauge transformations. The generalization of $U(1)$ to non-Abelian groups as $SU(N)$ is straightforward, the main modification arises in the definition of the field strength (21) that becomes $F_{\mu\nu} = \partial_\mu A_\nu - \partial_\nu A_\mu + [A_\mu, A_\nu]$. Since most of the gauge fields arising in the graphene context will not have dynamics we will not discuss this point further.

Einstein's General relativity can be also interpreted as a gauge theory where gauge invariance is invariance under diffeomorphisms (local smooth changes of coordinates) in the space-time manifold. The connection which generates parallel transport plays the role of the gauge field. The similarity is better appreciated in the vielbein formalism introduced in Section III C and Appendix 1 where a gauge transformation corresponds to a change of local frame (a local Lorentz transformation). Gauge invariance corresponds to the independence of field equations from the choice of the local frame. The spin connection plays the role of the gauge field.

In any gauge theory physical observables are related to gauge-invariant operators. The gauge invariance allows to fix some conditions on the gauge potentials that will not affect the physical properties. In quantum gauge theories gauge-fixing is a delicate issue that will no concern us here. In classical electromagnetism, the gauge-fixing problem is simply the problem of choosing a representative in the class of equivalent potentials, convenient for practical calculations or most suited to physical intuition. In non-relativistic problems one of the most popular choices is the Coulomb gauge: $\nabla \cdot \mathbf{A}(t, \mathbf{x}) = 0$ whose relativistic counterpart $\partial_\mu A^\mu(t, \mathbf{x}) = 0$, $\mu = (0, 1, 2, 3)$ is the Landau or Lorentz's gauge. The freedom to choose a gauge condition is related with the full gauge invariance of the action. When fictitious gauge fields are generated by analogy with the gauge formalism but there is no dynamics associated to them it can happen that the gauge potentials are fixed by the physics involved and no extra conditions can be imposed. A particular example is provided by the strain fields discussed in Sect. IV A. Gauge fields were introduced in condensed matter in the early works of refs. [59, 60].

D. Types of gauge fields

Different physical mechanisms give rise to perturbations in the Dirac equation described above which can be described mathematically as effective gauge fields. By definition, a gauge field appears in the off diagonal elements of the Dirac equation, which correspond to the hopping between sublattices. There are two ways in which this change in the hopping between sublattices can take place:

- The topology of the lattice itself can change, requiring a redefinition of the two sublattices. This happens in the presence of topological defects, such as pentagons and heptagons (disclinations), or pentagon-heptagon pairs (dislocations). If the carbon atoms remain with threefold coordination, the local electronic structure is not altered very much, and an effective Dirac equation can be defined locally. The defect changes the global properties of the lattice. Modifications of the internal degrees of freedom of the electrons when they propagate over long distances can be described by gauge fields, as defined more precisely in the following section.

The substitution of hexagons by rings with fewer or more sites, when the bond lengths remain more or less unchanged, leads to the curvature of the structure, according to Euler's theorem. As described below, these defects induce, in the continuum limit, the spin connection which modifies the Dirac equation of a spinorial field, extensively discussed in quantum field theory in curved spaces. Because these gauge fields arise from general topological features of the system, *these gauge fields do not depend on any material parameter.*

- The hopping between π orbitals in different sublattices can also change because the distance between the orbitals is modified, or because a change of symmetry allows for indirect hoppings through the σ orbitals [61], also present in the system. *These fields depend on microscopic details of the material.* The same changes in the electronic spectrum are induced when the atoms oscillate around their equilibrium positions, so that the parameters which describe the strength of these gauge fields contribute also to the electron-phonon coupling.

Small static deformations of the lattice are described by the strain tensor. A field with the symmetries of a vector can be obtained by contracting the strain tensor with a third rank tensor. The trigonal symmetry of the honeycomb lattice allows for such a third rank tensor[62, 63] (note that a vector gauge field cannot be defined in a fully isotropic system). The curvature away from the flat configuration can be described in a similar way by the curvature tensor. The induced gauge field in the Dirac equation is obtained in analogous way by contracting the curvature tensor and the third rank trigonal tensor described above.

III. TOPOLOGICAL DEFECTS IN GRAPHENE

As described in Sect. II A, graphene consists of a planar honeycomb lattice of carbon atoms determined by the sp^2 hybridization of the $2s$, $2p_x$ and $2p_y$ orbitals of the carbon system. These σ bonds give rigidity to the structure, while the π bonds give rise to the valence and conduction bands. The elastic properties of the material are related with the σ bonds and involve energies of the order of 7-10 eV similar to the bandwidth of graphene ($\sim 14eV$). The carbon bond in graphite is one of the strongest chemical bonds occurring in nature. The Young's modulus of graphene is of the order of $350 \text{ N} \cdot \text{m}^{-1}$, one of the highest values known for any material [64–66].

Topological defects in solids are usually described by complicated boundary conditions in elasticity theory. It was very early realized that they may be described more simply as sources of a gravity-like deformation [40]. In this approach the boundary conditions imposed by defects in elastic media are accounted for by introducing curvature in the given space. In the continuum limit the crystal is described by a manifold where curvature and torsion are associated to disclinations and dislocations in the medium respectively. The Burgers vector of a dislocation is

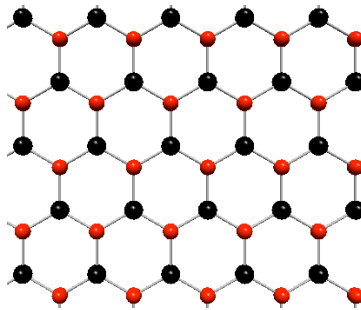


FIG. 2: (Color online) Honeycomb lattice of monolayer graphene.

associated to torsion, and the Frank angle of a disclination to curvature. The combined effect of curvature and elasticity has been studied in [67] and the scattering of phonons in the presence of a disclination and of multiple disclinations in [68]. The fact that elastic deformations of a crystal lattice induce gauge fields that couple to the electronic degrees of freedom has been known for a long time [36] and it has been applied to nanotubes and graphene in [41, 42, 68]. The mechanics of defects of various classes in graphene has been analyzed recently in [69]. The authors discuss the failure of classical elasticity to describe divacancies and Stone-Wales defects. The defect formation under strain was studied in the context of carbon nanotubes in [70].

A. Topological defects. Formation and naturalness

A very natural way of producing local curvature in the graphene lattice is by substituting some of the hexagons by pentagons (positive curvature) or heptagons (negative curvature). These types of topological defects are present in all the previously existing graphene structures (fullerenes and nanotubes), have been observed experimentally [71–73] and their elastic and electronic properties have been studied at length [74]. It is well known for instance from studies of stability of carbon nanotubes that vacancies and similar defects produced in the graphene structure by ion irradiation of the samples are mended by forming higher membered rings. Subsequently the unstable high-membered rings have been found to disappear by Stone-Wales transformations [75], thus leading to very stable structures mainly constituted of five-, six-, and seven-membered rings [76]. High-resolution Transmission Electron Microscopy (TEM) with atomic sensitivity reported the first direct imaging of pentagon–heptagon pair defects in a single wall carbon nanotube heated at 2,273 K in [77].

The recent TEM experiments performed in suspended graphene sheets [43, 44] seem to indicate that the observed structure can not be explained by strain-free deformations of graphene. Topological defects can be produced in the process of mechanical cleavage which involves quite high energies. They would induce strain-free curvature compatible with the experimental data. Although the observed tilt reported is argued to produce a strain too small to give rise to nucleations of defects [43], it can well be that the structure observed is the final result of a fully relaxed structure where high energy deformations have relaxed through formation of topological defects and the lower energy elastic deformations remain. Topological defects could also be preexisting in the underlying graphite material. Even if the observed structure in graphene is not due to these types of defects, it is worth to study how their presence would affect the electronic and elastic properties of the material. In terms of the elasticity theory the pentagons and heptagons represent disclinations of the lattice. Each disclination is made by either removing or inserting a wedge of material as shown in Fig. 4 for the particular case of a pentagon. Such a procedure would create an enormous elastic strain in flatland, i.e., if you insist in gluing the edges in flat space. The structure is much more - or fully - relaxed if the crystal is allowed to bend in the third direction forming a cone (or a saddle point structure in the case of excess angle). This procedure is not possible in three dimensional crystals where disclinations are very rare. A dislocation can be formed by joining a pentagon and a heptagon through a line which will represent the Burgess vector of the dislocation. The Stone-Wales defects [75] play a very important role in the structural stability of the previously existing graphene structures. They are formed by two pentagon-heptagon pairs oriented as displayed in Fig. 3 and are the result of a 90 degrees rotation of a bond in the honeycomb lattice. In terms of the elasticity theory they can be represented as two adjacent dislocations. The spontaneous formation of the Stone-Wales defects is known to be the main mechanism to relief strain in plastically deformed nanotubes [78].

The electronic properties of topological defects in graphene have been studied at length in the literature by applying various numerical methods [79–81]. The main founding is that they induce charge inhomogeneities in the samples

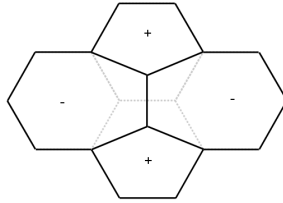


FIG. 3: A Stone-Wales defect is made by a 90 degrees rotation of a bond in the honeycomb lattice what produces two pentagon-heptagon rings.

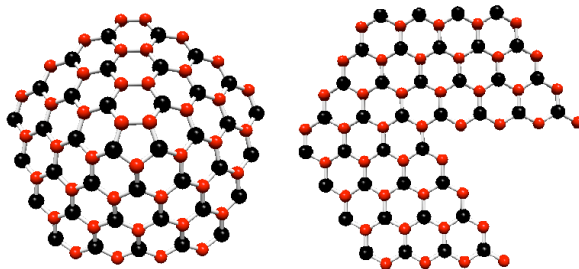


FIG. 4: (Color online) Left: Effect of a pentagonal defect in a graphene layer. Right: Cut-and-paste procedure to form the pentagonal defect. The points at the edges are connected by a link what induces the frustration of the bipartite character of the lattice at the seam (taken with permission from Ref. [88]).

with characteristic patterns that can be observed in STM and EFM experiments. Substitution of a hexagonal ring by odd-sided polygons break the electron-hole symmetry which is preserved by even-sided rings. Pentagonal rings have been suggested as excellent field emitters [82]. In the recent field of topological insulators [56, 57] topological defects are able to bind excitations with fractionalized quantum numbers [83, 84]. The tight-binding approach for graphene in the presence of pentagonal and heptagonal rings has been worked out in the context of nanotubes in the pioneer paper of ref. [85]. Analytical approaches give rise to the appearance of various gauge fields which we will review. An interesting question is whether these “plastic” deformations can be distinguished from the elastic deformations which also give rise to gauge fields in the continuum limit [36]. One of the main papers to address this issue that appeared again in the nanotube literature is [86]. It has also been discussed very recently in [87].

We will first review the case of disclinations where a hexagonal ring of the honeycomb lattice is replaced by either a pentagon or a heptagon. We will deal with the continuum model under the assumption that the electronic structure of graphene is well described by (two) massless Dirac equations in two space dimensions.

B. The gauge approach to disclinations

We will see that modelling disclinations in the continuum gives rise to three different gauge fields coupled to the electronic degrees of freedom. One is associated to the phase mismatch seen by the electron when circling around the defect (holonomy). This one is independent of the lattice structure and will take care of the conical shape of the graphene electron energy surfaces [48, 89–92]. The second class has to do with the frustration of the triangular sublattice ordering that occurs in the seam (see Fig. 4) and the exchange of the Fermi points that occurs when going around a pentagon or an heptagon. These effects were described in full detail in [48, 89] and can be modelled by non-Abelian gauge fields. Finally the presence of various defects forces the introduction of a third type of gauge field associated to the fact that the tight binding phase does not commute with the holonomy associated with the exchange of the Fermi points [49, 93, 94].

1. *Two gauge fields for a single disclination*

In relativistic quantum field theory where there is a very tight connection between the spin and the statistics, a spin 1/2 particle is described by a field that belongs to the so-called spinor representation of the Lorentz group. A distinct characteristic of spinor representations is that when they move around a closed path they pick up a minus sign (upon a 2π rotation they acquire a phase of π). A spinor going around a closed path encircling the pentagon in Fig. 4 will acquire a phase proportional to one half the total angle of the path $\phi = 2\pi(1 - 1/6)$. When solving the Schrödinger equation $H\Psi = E\Psi$ with the Hamiltonian (2) this condition has to be imposed on the wave function as a boundary condition which is often hard to deal with. A way to incorporate the constraint attached to the boundary condition to the Hamiltonian is to remind the Bohm-Aharonov (BA) effect and substitute the pentagon by a fictitious magnetic field located at the same point. The flux of the field can be adjusted so that the phase acquired by the spinor when going around the vector potential is the same as the one induced by going around the pentagon. This procedure has the advantage of being easily generalized to conical defects of arbitrary opening angle. In the BA effect the phase is proportional to the circulation of the vector potential along the closed path:

$$\oint \mathbf{A} \cdot d\mathbf{r} = 2\pi(1 - 1/6). \quad (25)$$

The simplest vector potential having the property (25) is a vortex:

$$\mathbf{A}(x, y) = \frac{5\pi}{3} \left(\frac{-y}{x^2 + y^2}, \frac{x}{x^2 + y^2} \right) = -\frac{5\pi}{3} \nabla\theta(r), \quad (26)$$

which in polar coordinates reduces to the gradient of the polar angle θ . The presence of a pentagon in the lattice has an additional consequence which was discussed at length in [89]: the two sublattices of black and white points are exchanged by going around a conical singularity, the admissible wave functions are made of pairs of plane waves with opposite momenta as described in Se. In momentum space the inversion with respect to the origin exchanges the two independent classes of Fermi points. It becomes clear that, for the mentioned honeycomb lattices, the states of the theory have to accommodate into the spectrum of two coupled Dirac spinors. This new condition can be fulfilled by attaching a quantum number (flavor) to the Fermi points, and considering the two bi-spinors $\psi_i(\mathbf{r})$, $i = +, -$ as the two components of an SU(2) flavor doublet. The vector field will now be a non-Abelian gauge field able to rotate the spinors in this flavor space. The full boundary condition to impose on the spinor when circling a pentagon (or any conical singularity of arbitrary defect angle φ) is

$$\begin{aligned} \Psi(\theta = 0) &= T_C \Psi(\theta = 2\pi) \Leftrightarrow \\ \Psi(\theta = 0) &= \exp\left(\oint_C \mathbf{A}_a T^a d\mathbf{r}\right) \Psi(\theta = 2\pi), \end{aligned} \quad (27)$$

$$\oint \mathbf{A} \cdot d\mathbf{r} = 2\pi - \varphi.$$

where \mathbf{A}_a are a set of gauge fields and T^a a set of matrices related to the flavor SU(2) degree of freedom of the system. In this way we end up with the Dirac equation coupled to a gauge potential:

$$H = -i\hbar v_F \vec{\gamma} \cdot \vec{\partial} + g \gamma^q \vec{\gamma} \cdot \vec{A}(\mathbf{r}), \quad (28)$$

where v_F is the Fermi velocity, γ^q is a 4×4 matrix constructed from the Pauli matrices chosen so as to accomplish the gauge transformation produced by the given defect, the Latin indices run over the two spatial dimensions and g is a coupling parameter. The external field $A_i(\vec{r})$ takes the form of a vortex

$$A^j(\vec{r}) = \frac{\Phi}{2\pi} \epsilon^{3ji} \frac{x_i}{r^2}, \quad (29)$$

and the constant Φ is a parameter that represents the strength of the vortex: $\Phi = \oint \vec{A} d\vec{r}$ and is related to the opening angle of the defect.

Since disclinations corresponding to even-sided polygons do not frustrate the sublattice symmetry, the associated matrix γ^q in eq. (28) for this case is

$$\gamma^q = \frac{\sigma_3}{2} \otimes I. \quad (30)$$

2. *Generalization to several defects: gauge fields arising from the holonomy*

A generalization of the gauge approach to include various topological defects was presented in [49, 92, 93]. The strategy consists of determining the phase of the gauge field by parallel transporting the state in suitable form along a closed curve surrounding all the defects.

$$\begin{aligned} \Psi(\theta = 0) &= T_C \Psi(\theta = 2\pi) \\ \Leftrightarrow \Psi(\theta = 0) &= \exp\left(\oint_C \mathbf{A}_a T^a d\mathbf{r}\right) \Psi(\theta = 2\pi), \end{aligned} \quad (31)$$

where \mathbf{A}_a are a set of gauge fields and T^a a set of matrices related to the pseudospin degrees of freedom of the system.

When dealing with multiple defects, we must consider a curve surrounding all of them, as the one sketched in Fig. 5.

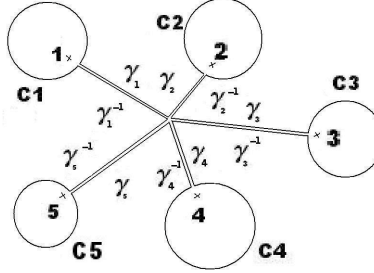


FIG. 5: Scheme of a prototypical curve enclosing multiple defects in which the state will be parallel transported.

The contour C is made of closed circles enclosing each defect and straight paths linking all the contours to a fixed origin. The parallel transport operator P_C associated to the closed path is thus a composition of transport operators over each piece:

$$P = P_{\gamma_1} \cdot P_1 \cdot P_{\gamma_1}^{-1} \cdot \dots \cdot P_{\gamma_N} \cdot P_N \cdot P_{\gamma_N}^{-1}, \quad (32)$$

where P_i is the phase associated with going around a single defect discussed in the previous subsection and P_{γ_i} is the chiral phase acquired by the wave function while travelling in the straight paths and depends on the distances (n, m) between defects.

The total holonomy turns out to be

$$\begin{aligned} P &= (i)^N (\tau_2)^N \exp\left(\frac{2\pi i}{6} (N^+ - N^-) \sigma_3\right) \cdot \\ &\quad \exp\left(\frac{2\pi i}{3} \sum_{j=1}^N (n_j - m_j) \tau_3\right), \end{aligned} \quad (33)$$

where N is the total number of defects equal to the sum of pentagons (N_+) and heptagons (N_-), and (n, m) is the position of the given defect in the usual chiral basis for the graphene lattice. Then we see that in the modelling of disclinations with the gauge approach described in this section there appear three different gauge fields to incorporate to the Dirac equation, which couple to the matrices σ_3 , τ_2 and τ_3 :

1. Gauge fields due to the holonomy: deal with the deficit or surplus of graphene slices

$$\Lambda_\sigma = \exp(-i\pi\sigma_3/6).$$

This boundary condition only affects the AB pseudo-spin structure.

2. The second type deals with the identification of the two sublattices

$$\Lambda_\tau = \exp(i\pi\tau_2/2).$$

This part of the boundary condition affects the valley (K, K') structure of the spinor: the two conical points are intertwined.

3. A third holonomy appears when more than one defect is considered:

$$\Lambda_3 = \exp\left(\frac{2\pi i}{3} \sum_{j=1}^N (n_j - m_j) \tau_3\right).$$

This boundary condition comes from the fact that the tight binding phase does not commute with the holonomy associated with τ_2 .

From (33) it is easy to see that for a Stone-Wells defect we have $N_+ = N_- = 2$, $n_i = m_i = 1$ and $\sigma_2^4 = 1$ and hence there is no gauge field associated to it. This casts some doubts on the completeness of the gauge description as it is known that such a defect alters the electronic structure of the graphene sheet [50, 88]. In the next section we will see that curvature effects account for the missing piece.

C. Modelling curvature. Dirac fermions in curved space

Many of the unusual properties of graphene arise from the fact that its quasiparticles are described by Dirac spinors. The special structure of the spinors is linked in particular to the Klein paradox and to the absence of back scattering in the samples [25]. When trying to study the possible consequences of the ripples found in the samples on the electronic properties it looks very natural to use the formalism of quantum field theory in curved spaces [95]. The main justification to use this approach is the robustness of the Dirac description versus deformations of the underlying lattice described in Section IIB. We must notice that, although the formalism is similar to that used in general relativity, here the geometry (curvature) of the space is fixed and the description is purely geometrical: the aim is to construct a Hamiltonian with scalar quantities made out of vectors or spinors in a curved background. This approach was applied to study the electronic spectrum of the fullerenes in [48, 67, 89, 93, 96]. A somehow similar approach is used in [97] in the framework of the equivalence between the theory of defects in solids and the three-dimensional gravity [40] to study the response of electromagnetic charges to conical defects in planar graphene. The geodesic around a dislocation has been treated in [98]. The coupling of the electronic degrees of freedom of planar graphene to conical defects within the geometric formalism has been explored in [50, 88, 94, 99]. There it was found that a distribution of pentagons and heptagons induces characteristic inhomogeneities in the density of states of the graphene surface. It was shown that the charge density was enhanced around the pentagonal defects and depressed near the heptagons, a result that was also predicted earlier in numerical calculations [79]. The effect was very localized and disappeared a few lattice constants away from the defect.

In order to investigate the effect of pure curvature on the electronic properties of graphene, the conical defects studied previously present two difficulties. First, they correspond to surfaces with zero intrinsic curvature; moreover, the extrinsic curvature is accumulated at the apex of the cone where the surface has a singularity. It is then not clear if the results obtained – which look similar to the ones got with vacancies in [100] – are due to the singularity or to the curvature. To disentangle the two effects a flat graphene sheet with a smooth curved portion with intrinsic curvature was analyzed in [101]. In all cases the curvature gives rise to gauge fields with a derivative coupling. In what follows we will sketch the formalism and give a summary of the results obtained so far within the geometric approach. A derivation of the main geometrical factors associated to the formalism is given in Appendix A.

The dynamics of a massless Dirac spinor in a curved spacetime with the metric tensor $g^{\mu\nu}$ is governed by the modified Dirac equation:

$$i\gamma^\mu(\mathbf{r})\nabla_\mu\psi = 0. \quad (34)$$

The two geometric objects entering the Dirac equation are the Pauli (gamma) matrices and the derivative of the spinor field. Both are vectors that need to be properly defined in a curved space. The curved space γ matrices must obey the generalized anticommutation relations:

$$\{\gamma^\mu(\mathbf{r}), \gamma^\nu(\mathbf{r})\} = 2g^{\mu\nu}(\mathbf{r}),$$

and become functions dependent on the point of the space. They are related to the constant flat matrices through the “vielbeins” described in the Appendix A. The covariant derivative operator is defined as

$$\nabla_\mu = \partial_\mu - \Gamma_\mu$$

where Γ_μ is the spin connection of the spinor field whose detailed construction is also given in the Appendix A.

Once the metric of the curved space is known there is a standard procedure to get the geometric factors that enter into the Dirac equation. In the modelling of the graphene ripples, the metric can be treated as a smooth perturbation

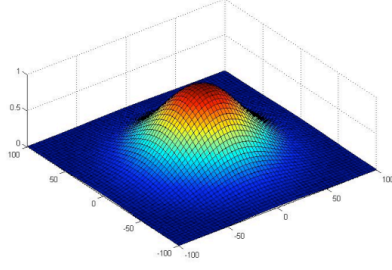


FIG. 6: (Color online) A smooth curved bump in the graphene sheet (taken with permission from Ref. [101]).

of the flat surface and physical results are obtained by a kind of perturbation theory. Very often, the final result can be casted in the form of the flat Dirac problem in the presence of a potential induced by the curvature. In ref. [101] a smooth general metric was considered of which an example is given by the gaussian shape of Fig. 6. A simple way to derive the metric of a smooth shape (spherically symmetric for convenience) is as follows: Start by embedding a two-dimensional surface with polar symmetry in three-dimensional space (described in cylindrical coordinates). The surface is defined by a function $z(r)$ giving the height with respect to the flat surface $z = 0$, and parametrized by the polar coordinates of its projection onto the $z = 0$ plane. To obtain the metric we compute

$$dz^2 = \left(\frac{dz}{dr} \right)^2 dr^2 \equiv \alpha f(r) dr^2, \quad (35)$$

and substitute for the line element:

$$ds^2 = dr^2 + r^2 d\theta^2 + dz^2 = (1 + \alpha f(r)) dr^2 + r^2 d\theta^2. \quad (36)$$

For the particular example of the gaussian bump given in Fig. 6: $z = A \exp(-r^2/b^2)$, the line element reads:

$$ds^2 = -(1 + \alpha f) dr^2 - r^2 d\theta^2, \quad (37)$$

where α is the ratio of the height to the mean width of the gaussian that can be used as a perturbative parameter over the flat case. The metric (37) can be written in a more usual form:

$$g_{\mu\nu} = \begin{pmatrix} -(1 + \alpha f(r)) & 0 \\ 0 & -r^2 \end{pmatrix}. \quad (38)$$

Comparing the flat Hamiltonian written in polar coordinates:

$$H_{flat} = \hbar v_F \begin{pmatrix} 0 & \partial_r + i \frac{\partial_\theta}{r} + \frac{1}{2r} \\ \partial_r - i \frac{\partial_\theta}{r} + \frac{1}{2r} & 0 \end{pmatrix}, \quad (39)$$

with the curved Hamiltonian

$$H_{curved} = \hbar v_F \begin{pmatrix} 0 & (1 + \alpha f(r))^{-1/2} \partial_r + i \frac{\partial_\theta}{r} + A_\theta \\ (1 + \alpha f(r))^{-1/2} \partial_r - i \frac{\partial_\theta}{r} + A_\theta & 0 \end{pmatrix}, \quad (40)$$

it can be seen that the curved bump induces an effective Fermi velocity \tilde{v}_r in the radial direction given by

$$\tilde{v}_r(r, \theta) = v_F (1 + \alpha f(r))^{-1/2}, \quad (41)$$

and an effective magnetic field perpendicular to the graphene sheet given by

$$B_z = -\frac{1}{r} \partial_r (r A_\theta) = \frac{1}{4r} \frac{\alpha f'}{(1 + \alpha f)^{3/2}}. \quad (42)$$

The magnitude of this effective magnetic field is estimated to be of the order of 0.5 to 2-3 Tesla in the region spanned by the bump, compatible with the estimations given in [41], and it plays the same role in the issue of the weak localization of graphene as the effective magnetic fields discussed there and in [42].

To first order in the perturbative parameter α the effective potential that appears in the Dirac equation in polar coordinates is

$$V(r, \theta) = i\Gamma(\theta) \left[\frac{1}{2} \alpha f(r) \right] \left(\frac{1}{2r} - \partial_r \right). \quad (43)$$

The physical properties of the system are obtained from the Green's function in the curved space as explained in Section V B.

The metric approach was used to describe topological defects in [50]. The proposed metric was as a generalization to the one used to model cosmic strings [102]:

$$ds^2 = -dt^2 + e^{-2\Lambda(x,y)}(dx^2 + dy^2), \quad (44)$$

where

$$\Lambda(\mathbf{r}) = \sum_{i=1}^N 4\mu_i \log(r_i),$$

μ_i is related to the defect angle of the disclination. In the case of having heptagonal defects with an “excess” angle, the sign of μ_i is negative. Here

$$r_i = [(x - a_i)^2 + (y - b_i)^2]^{1/2},$$

where (a_i, b_i) are the positions of the defects. The curved space formalism applied to this geometry induces an effective potential:

$$V(\omega, \mathbf{r}) = 2i\Lambda\gamma^0\partial_0 + i\Lambda\gamma^j\partial_j + \frac{i}{2}\gamma^j(\partial_j\Lambda), \quad (45)$$

which gives rise to spacial inhomogeneities in the local density of states as discussed in Section V. The fictitious gauge field coming from the spin connection is similar to the one encountered in elasticity formalisms. A distinctive feature of the covariant approach is the space dependent coefficient in the kinetic term of the effective Hamiltonian that can be interpreted as a space-dependent Fermi velocity that could eventually be used to test the validity of the model. The influence of this extra term on the minimal conductivity has been analyzed in [103].

D. The electronic spectrum of fullerenes

The ideas of modelling conical defects by gauge fields and adding geometric curvature were established in the early publication [89] where they were applied to compute the electronic spectrum of the spherical fullerenes. The most popular of them, the “buckyball” C_{60} has the shape of a soccer ball, consisting of 12 pentagons and 20 hexagons. The structure is that of a truncated icosahedron. There is a full set of fullerenes of the same symmetry consisting of adding crowns of hexagons around the pentagons. Following the analysis described before, modelling the C_{60} molecule can be done with 12 non-Abelian vortices that would account for both the singular curvature, and the exchange of the Fermi points associated to the pentagons. Given the compact nature of the system, the model proposed in [89] was to solve the Dirac equation on the surface of a sphere with a fictitious magnetic monopole at its center. The sphere smears the curvature accumulated at each pentagon, and the charge g of the fictitious magnetic monopole is adjusted by adding up the individual fluxes of all the lines:

$$g = \frac{1}{4\pi} \sum_{i=1}^N \frac{\pi}{2} = \frac{N}{8}, \quad (46)$$

N being the number of conical singularities on the surface. It is interesting to note that the value of g required for the icosahedron ($N = 12$), $g = 3/2$, is compatible with the standard quantization condition of the monopole charge.

The given model reproduces the low-energy spectra and correct numbers of zero modes for the C_{60} family of fullerenes and works better in the limit of large number of points. The spectrum is obtained by solving the eigenvalue problem for the covariant Dirac operator

$$i\sigma^a e_a^\mu (\nabla_\mu - iA_\mu)\Phi_n = \epsilon_n \Phi_n, \quad a, \mu = 1, 2, \quad (47)$$

where e_μ^a is the zweibein for the sphere, and the geometrical factors in spherical coordinates are

$$\nabla_\theta = \partial_\theta,$$

$$\nabla_\phi = \partial_\phi - \frac{1}{4}[\sigma^1\sigma^2]\cos\theta,$$

$$A_\theta = 0,$$

$$A_\phi = g \cos\theta \tau^{(2)}.$$

The Dirac equation becomes

$$\begin{aligned} \frac{v_F}{R} \left[i\partial_\theta - \frac{1}{\sin(\theta)}\partial_\phi + \frac{i(1+g)}{2\cos(\theta)}2\sin(\theta) \right] \Psi_1(\theta, \phi) &= E\Psi_2(\theta, \phi) \\ \frac{v_F}{R} \left[i\partial_\theta + \frac{1}{\sin(\theta)}\partial_\phi + \frac{i(1-g)}{2\cos(\theta)}2\sin(\theta) \right] \Psi_2(\theta, \phi) &= E\Psi_1(\theta, \phi) \end{aligned} \quad (48)$$

where R is the radius of the sphere.

The Dirac equation can be diagonalized by introducing a generalized angular momentum operator \mathbf{J} taking into account spinor indices, magnetic field and curvature. We find

$$\begin{aligned} J^+ &= e^{i\phi}\partial_\theta + ie^{i\phi}\frac{\cos(\theta)}{\sin(\theta)}\partial_\phi + e^{i\phi}\frac{g-1}{2\sin(\theta)} \\ J^- &= -e^{-i\phi}\partial_\theta + ie^{-i\phi}\frac{\cos(\theta)}{\sin(\theta)}\partial_\phi + e^{-i\phi}\frac{g-1}{2\sin(\theta)} \\ J_z &= -i\partial_\phi \end{aligned} \quad (49)$$

By squaring the Dirac operator each of the spinor components obeys the equation

$$E_J^2 = \left(\frac{v_F}{R}\right)^2 \left(J(J+1) + \frac{1}{4} - g^2 \right) \quad (50)$$

where J is the eigenvalue of the angular momentum, which is an integer. The degeneracy of a state is $2J+1$. From Eq. (50) it can be seen that there is minimum value of the angular momentum J dictated by g , so that the number of zero modes in the spectrum depends exclusively on the value of the monopole charge, i. e. on the number of pentagons in the lattice. It is also interesting to note that, since the sphere has a constant curvature, there are no inhomogeneous geometrical factors and all the effect of the curvature reduces to a rescaling of the energy. Substituting $g = 3/2$ in Eq. (50) gives the spectrum of the C_{60} family of fullerenes: the ground state is a couple of triplets lying at zero energy, and the first excited levels follow the degeneracy of the sphere up to the point in which the highest dimension of an irreducible representation of the icosahedron symmetry group is reached. The model works very good given its simplicity. The elastic properties of the fullerenes were analyzed within this approach in [48].

E. Dislocations and torsion: a general relativity approach

The gravity connection can be pushed forward and used to model a density of dislocations in the space in the continuum limit by adding torsion to the space spanned by the lattice. The connection of torsion with the continuum theory of crystal dislocations goes back to Kondo [104] and has been formalized in [36, 40]. Various aspects of the problem have been explored in [105]. A nice review on the relation of gravity with topological defects in solids is [106]. The geometric approach to defects in solids [36, 107] relates the metric of the curved crystalline surface with the deformation tensor and establishes that disclinations are associated to the curvature tensor and a finite density of dislocations generates a torsion term.

Dislocations in graphene are made of pentagon–heptagon pairs and they have been widely studied in connection with the properties of carbon nanotubes [74] and, more recently, in the flat graphene sheets or ribbons [108, 109]. The covariant approach described above was extended in [110] to include a connection with torsion. As we discussed

in Section IID the minimal coupling of any geometrical or physical fields to the Dirac spinors adopts always the form of a covariant derivative:

$$\partial_\mu \Rightarrow D_\mu = \partial_\mu + A_\mu, \quad (51)$$

where the given vector can be an electromagnetic potential induced by a real electromagnetic field or any other real or fictitious gauge field associated to deformations or to geometrical factors. In the case of having a density of dislocations in the graphene sheet modelled by torsion we can construct two potential candidates to gauge fields:

$$V_\mu = g^{\nu\rho} T_{\nu\rho\mu}, \quad S_\mu = \epsilon_{\mu\nu\rho\sigma} T_{\nu\rho\sigma}, \quad (52)$$

where $T_{\mu\nu\rho}$ is the rank three torsion tensor related to the antisymmetric part of the connection:

$$T_{\mu\nu}^\lambda = \Gamma_{\mu\nu}^\lambda - \Gamma_{\nu\mu}^\lambda. \quad (53)$$

The field V_μ is an ordinary vector and can be associated to the density of edge dislocations while S_μ is an axial (pseudo) vector associated to the density of screw dislocations.

IV. STRAIN FIELDS

A. Modulations of the tight binding parameters

In this section we will consider gauge fields which arise in defect-free graphene due to smooth elastic deformations. The latter can be created by applying external stress to graphene flakes. It is important to notice that these deformations and the related gauge fields are also intrinsic for graphene at finite temperatures due to thermal fluctuations (see Section IV D). These gauge fields were discussed in a context of electron-phonon interactions in nanotubes prior to the synthesis of graphene in [62, 111].

Let us start with a tight-binding model of the electronic structure of graphene in the nearest-neighbor approximation. In the deformed graphene all bonds are, in general, nonequivalent and the three nearest-neighbors hopping parameters t_i can be all different. If one repeats the derivation of the Dirac Hamiltonian in the effective mass approximation but with nonequal hopping parameters one finds for the electron states in the vicinity of the K point the effective Hamiltonian:

$$H = -i\hbar v_F \vec{\sigma} \left(\vec{\nabla} - i\vec{A} \right), \quad (54)$$

where [27, 62, 111]

$$\begin{aligned} A_x &= \frac{\sqrt{3}}{2} (t_3 - t_2), \\ A_y &= \frac{1}{2} (t_2 + t_3 - 2t_1), \end{aligned} \quad (55)$$

(note that, following Ref. [62] and most of the subsequent works, we use a choice of the axes x, y different from that made in Refs. [27, 111]). In the weakly deformed lattice, assuming that the atomic displacements \vec{u} are small in comparison with the lattice constant a one has

$$t_i = t + \frac{\beta t}{a^2} \vec{\rho}_i \cdot (\vec{u}_i - \vec{u}_0), \quad (56)$$

where $\vec{\rho}_i$ are the nearest-neighbor vectors, \vec{u}_0 is the displacement vector for the central atom, and

$$\beta = -\frac{\partial \ln t}{\partial \ln a} \simeq 2 \quad (57)$$

is the electron Grüneisen parameter (for more details, see below). The continuum limit (elasticity theory) with a displacement field $\vec{u}(\vec{r})$ is performed by making the substitution

$$\vec{u}_i - \vec{u}_0 \propto (\vec{\rho}_i \cdot \nabla) \vec{u}(\vec{r}), \quad (58)$$

from where we obtain the effective gauge field [62, 63]:

$$\begin{aligned} A_x &= c \frac{\beta t}{a} (u_{xx} - u_{yy}), \\ A_y &= -c \frac{2\beta t}{a} u_{xy}, \end{aligned} \quad (59)$$

where c is a numerical factor depending on the detailed model of chemical bonding; in what follows we will make our estimations with the value $c = 1$.

For the other valley, K' , the sign of the vector potential (59) is opposite, in agreement with the requirement of time-reversal invariance. Indeed, atomic displacements can break effectively the time-reversal symmetry (involving inversion of the wave vector) for a given valley but not for the crystal in general.

If the deformation is not a pure shear and the dilatation does not obey the condition $\nabla \vec{u} = u_{xx} + u_{yy} = 0$, a scalar potential proportional to $\nabla \vec{u}$ also arises [62]. The gauge field (59) is proportional to the deformation tensor which is directly involved in the density of elastic energy (see the next Section). This means that the problem as a whole is *not* gauge invariant. For example we could add to the gauge potential the gradient of a scalar function and shift the electronic wave function by a phase as discussed in Section II C leaving the electronic part of the Lagrangian invariant but these transformations will change the elastic part. The simplest argument to understand this lack of gauge invariance is to notice that the kinetic energy term for the elastic part is isotropic (see Eq. (62)) while the effective vector field given by Eq. (59) is not.

On general symmetry grounds, strains can also lead to scalar potential[62, 63],

$$V(\vec{r}) = g(u_{xx} + u_{yy}) \quad (60)$$

This term enters in the diagonal elements of the Dirac equation. The most recent calculations suggest that $g \approx 4\text{eV}$ for a neutral graphene single layer[112], although higher values, $g \approx 20\text{eV}$ have been cited in earlier literature[62, 113, 114]. The parameters β and g describe the coupling to acoustical in graphene, and they are usually considered simultaneously, as they both contribute to the deformation potential, D . Combinations of the type $D^2 = c_1 \times (v_F^2 \beta^2)/a^2 + c_2 \times g^2$, where c_1 and c_2 are numerical constants determine the phonon contribution to transport coefficients, like the resistivity. Microscopic models for the deformation potential have considered only the effect of the gauge potential[115–118], or both the scalar and gauge potentials[119].

B. Gauge fields as function of the in plane strains

Long wavelength distortions within the graphene layers can be described using the strain tensor[120], $u_{\alpha\beta}$. This tensor defines the local deformation of the lattice. Given the deformation field $\vec{u}(x, y)$, the strain tensor in the linear approximation is:

$$u_{\alpha\beta} = \frac{\partial_\alpha u_\beta + \partial_\beta u_\alpha}{2}. \quad (61)$$

The elastic energy is:

$$E_{elas} = \frac{\lambda}{2} \int d^2\vec{r} (u_{xx} + u_{yy})^2 + \mu \int d^2\vec{r} (u_{xx}^2 + u_{yy}^2 + 2u_{xy}^2), \quad (62)$$

where λ and μ are the elastic Lamé coefficients. We can also define the stress tensor, $\sigma_{\alpha\beta} = \partial E_{elas}/\partial u_{\alpha\beta}$,

$$\begin{aligned} \sigma_{xx} &= \lambda(u_{xx} + u_{yy}) + 2\mu u_{xx} \\ \sigma_{yy} &= \lambda(u_{xx} + u_{yy}) + 2\mu u_{yy} \\ \sigma_{xy} &= 2\mu u_{xy}. \end{aligned} \quad (63)$$

As discussed in Section II D, strains modify the bond lengths and the hopping between π orbitals. The dependence of the hopping on the interatomic distance is approximately the same in the organic compounds with sp^2 coordination, and it is parametrized by the dimensionless constant β (57). A change in the hopping between nearest neighbor atoms modifies the terms in the Hamiltonian which couple the two sublattices. In the previous section this was done explicitly, in the nearest-neighbor approximation. Actually, the expression (59) is more general. In the continuum limit, this coupling must take the form of a gauge field with the matrix structure of the Pauli matrices, σ_1 and σ_2 . A vector can be constructed from the strain tensor by contracting it with a rank three tensor. This tensor should be

invariant under the discrete set of symmetries of the honeycomb lattice. The only possible tensor with these properties has the non zero components:

$$\begin{aligned} K_{xxx} &= 1 \\ K_{yyx} &= K_{yxy} = K_{xyy} = -1, \end{aligned} \quad (64)$$

where the x axis coincides with one of the unit vectors of the lattice. The same tensor describes the first deviation from complete isotropy in the bands of the electrons in the honeycomb lattice, the so called trigonal warping [19].

From Eq. (64) it can be seen that the gauge field must take the form (59).

The combination of strains which enter in the gauge field, Eq. (59), can also be written in terms of the stress tensor, σ_{ij} :

$$\begin{aligned} u_{xx} - u_{yy} &= \frac{\sigma_{xx} - \sigma_{yy}}{2\mu} \\ 2u_{xy} &= \frac{2\sigma_{xy}}{2\mu}, \end{aligned} \quad (65)$$

where μ is a Lamé coefficient (shear modulus).

The calculation of the strains in a two dimensional system with only in-plane displacements is drastically simplified in comparison with a generic three dimensional case, as the stresses can be written in terms of a function [120]:

$$f(x, y) = \text{Re}[(x - iy)g(x + iy) + h(x + iy)], \quad (66)$$

where $g(z)$ and $h(z)$ are analytic functions of $z = x + iy$. The stress tensor is:

$$\begin{aligned} \sigma_{xx} &= \frac{\partial^2 f}{\partial y^2} \\ \sigma_{yy} &= \frac{\partial^2 f}{\partial x^2} \\ \sigma_{xy} &= -\frac{\partial^2 f}{\partial x \partial y}. \end{aligned} \quad (67)$$

A pure shear deformation has $\sigma_{xx} = -\sigma_{yy}$, which implies that $g(z) = 0$. Then we get the effective gauge potential:

$$\begin{aligned} A_x &\propto \text{Re}[h''(z)] \\ A_y &\propto \text{Im}[h''(z)], \end{aligned} \quad (68)$$

and the effective magnetic field is:

$$B = -\partial_y A_x + \partial_x A_y \propto \text{Im}[h'''(z)]. \quad (69)$$

A pure shear deformation that leads to a constant effective magnetic field is given by $h(z) = Az^3$, where A is a constant. A general deformation which satisfies the equilibrium equations of elasticity and which leads to a constant effective gauge field is determined by the function $f(z) = Az^3 + B\bar{z}z^2$.

A constant effective magnetic field requires a strain tensor which increases linearly with position, $u_{ij} = \bar{u}(\vec{r}\vec{n})/L$, where \vec{n} is a given unit vector, and L is the size of the system. The maximum stresses are of order \bar{u} . The effective magnetic field has an associated magnetic length:

$$\frac{1}{l_B^2} \approx \beta \frac{\bar{u}}{aL}, \quad (70)$$

where a is the lattice constant. For $\bar{u} = 0.01$ and $L = 1\mu\text{m}$ we obtain $l_B \approx 10^2\text{nm}$, which corresponds to a magnetic field of 0.5T. A description of the strains and effective fields induced by displacements with radial symmetry is given in the Appendix B.

C. Out of plane displacements

When the layer can be distorted along the out of plane direction, the strain tensor becomes:

$$u_{\alpha\beta} = \frac{\partial_\alpha u_\beta + \partial_\beta u_\alpha}{2} + \frac{\partial_\alpha h \partial_\beta h}{2}, \quad (71)$$

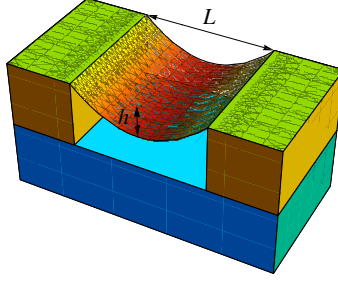


FIG. 7: Sketch of a suspended rectangular flake.

where h is the displacement along the third dimension. The distortion of the bonds is proportional to the square of h .

The simplest and most ubiquitous deformation expected in suspended graphene is due to the force induced by the electric field between the gate and the flake [121]. The total energy of a monolayer flake under a constant vertical force, as function of the maximum vertical deformation, h , can be written as [120]:

$$E_{tot} = E_{bend} + E_{elas} + E_{field} \approx c_{bend}\kappa \frac{h^2}{L^2} + (c_\lambda\lambda + c_\mu\mu) \frac{h^4}{L^2} + c_{field}\mathcal{F}hL^2, \quad (72)$$

where c_{bend} , c_λ , c_μ and c_{field} are numerical constants, $\kappa \approx 1$ eV is the bending rigidity of the flake, $\lambda \approx 2.4$ eV \AA^{-2} and $\mu \approx 9.9$ eV \AA^{-2} are the in plane elastic Lamé coefficients [66], and $\mathcal{F} = 2\pi e^2 n^2$ is applied field, and n is the carrier density that it induces. The bending energy in Eq. (72) is negligible with respect to the in plane elastic energy for $h \gtrsim \sqrt{\kappa/\max(\lambda, \mu)} \approx 1 - 3\text{\AA}$. Neglecting it, we obtain:

$$h \approx CL \left(\frac{e^2 n^2 L}{\max(\lambda, \mu)} \right)^{1/3}, \quad (73)$$

where C is a numerical constant which depends on details of the shape of the flake, and the ratio λ/μ . The neglect of the bending energy is justified for $n^2 L^4 \gtrsim \sqrt{\kappa^3/[e^4 \max(\lambda, \mu)]} \approx 0.1$. As $N = nL^2$ is the total number of carriers in the flake, the bending energy can be neglected in all realistic situations. For $n \sim 10^{12}\text{cm}^{-2}$ and $L \sim 1\mu\text{m}$, we obtain $h \sim 30\text{nm}$.

The strains associated to the deformation in Eq. (73) are of order:

$$u_{\alpha\beta} \sim (\nabla h)^2 \sim C \left(\frac{e^2 n^2 L}{\max(\lambda, \mu)} \right)^{2/3}, \quad (74)$$

leading to an effective magnetic field characterized by a magnetic length, l_B :

$$\frac{1}{l_B^2} \sim \frac{C}{\beta} aL \left(\frac{e^2 n^2 L}{\max(\lambda, \mu)} \right)^{2/3}, \quad (75)$$

where a is the lattice constant. For $n \approx 10^{12}\text{cm}^{-2}$ and $L \approx 1\mu\text{m}$, we obtain $l_B \sim 30 - 100\text{nm}$, which corresponds to effective fields of 2 – 10T.

The effective magnetic field is determined by the full strain tensor, which includes a contribution from the in plane displacements [122]. If the height profile, $h(\vec{r})$, is known, we can define:

$$f_{i,j}(\vec{r}) = \frac{\partial h}{\partial r_i} \frac{\partial h}{\partial r_j}. \quad (76)$$

Then, the Fourier component of the effective field, including the effect of the in plane strains can be written as:

$$B(\vec{k}) \propto ik_y \frac{(3k_x^2 - k_y^2)(\lambda + \mu)}{(\lambda + 2\mu)|\vec{k}|^4} \left[k_y^2 f_{xx}(\vec{k}) + k_x^2 f_{yy}(\vec{k}) - 2k_x k_y f_{xy}(\vec{k}) \right], \quad (77)$$

where \vec{k} is the wave vector. These corrections do not change the earlier order of magnitude estimates for the effective field, except in cases with high symmetry. For instance, when h is constant along one direction, i. e. y , the relaxation of the in plane displacements lead to a stress tensor such that $\sigma_{xx} = \text{constant}$, $\sigma_{yy} = \sigma_{xy} = 0$, and to a constant effective gauge field.

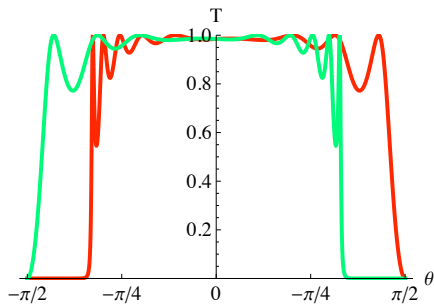


FIG. 8: Transmission through a suspended rectangular flake as function of incident angle. The carrier density is $\rho = 10^{12} \text{cm}^{-2}$, the length of the flake is $L = 100 \text{nm}$, and the maximum deformation is $h_0 = 3 \text{nm}$. Red and green lines correspond to the two valleys in the Brillouin Zone (see text for details).

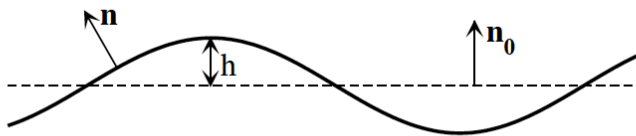


FIG. 9: Sketch of a flexible membrane (solid line). h is the out of plane deviation with respect to the $z = 0$ plane (dashed line) defined by the center of mass. The unit vector \mathbf{n} and \mathbf{n}_0 are the normals to each point in the membrane and in the reference plane respectively.

D. Thermal fluctuations and intrinsic ripples in graphene

From the general analysis of the previous sections it follows that corrugations of graphene with spatial scale much larger than the interatomic distance a lead to the formation of an Abelian gauge field. It turns out that for two-dimensional crystals at finite temperatures the corrugations are unavoidable, due to the instability of the crystal with respect to the bending fluctuations. In this section we will review the corresponding theoretical results.

The standard theory of lattice dynamics and thermodynamics [123] starts with the assumption that typical amplitudes of atomic displacements u due to thermal fluctuations are small in comparison with the interatomic distances, $\langle u^2 \rangle \ll a^2$. It was understood as early as in 1930th [1, 124–126] that for two-dimensional crystals at finite temperatures this cannot be the case, due to the logarithmic divergence of $\langle u^2 \rangle$. This has given rise to the hypothesis that long-range crystal order cannot exist in two dimensions which has been proven later, as a particular case of Mermin-Wagner theorem [127]. Therefore the experimental realization of graphene and other truly two-dimensional crystals [12, 13] was really surprising. The point is that these objects are not two-dimensional crystals in two-dimensional space but two-dimensional crystals in three-dimensional space; it follows from a general theory of flexible membranes [128] that such systems can exist but cannot be really flat [17, 43]. Very soon after the synthesis of graphene corrugations of freely suspended graphene membrane were observed experimentally [43]; the existence of intrinsic ripples in graphene due to thermal instability has also been confirmed by atomistic Monte Carlo simulations [129].

Let us start with the model of a continuum infinitely thin membrane (Fig. 9). It is characterized by the dependence of out-of-plane deformation on coordinates, $h(x, y)$. The normal vector to the membrane at a given point has components [128]

$$\mathbf{n}(x, y) = \frac{\left(-\frac{\partial h}{\partial x}, -\frac{\partial h}{\partial y}, 1\right)}{\sqrt{1 + |\nabla h|^2}}. \quad (78)$$

For liquid membranes, according to the Helfrich model [130, 131] the density of elastic energy contains two terms,

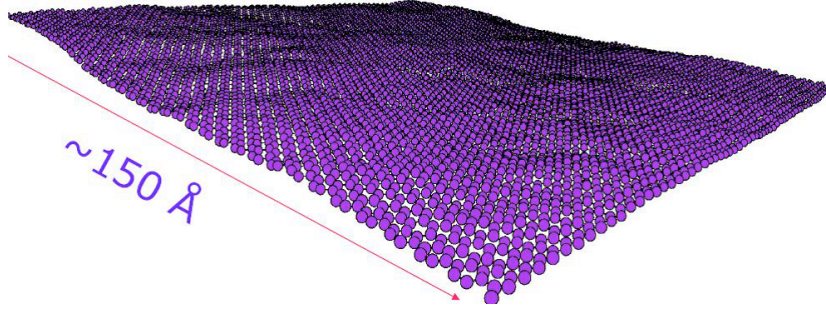


FIG. 10: A representative atomic configuration in Monte Carlo simulations [129, 133] for graphene at room temperature (courtesy A.Fasolino).

proportional to the square of mean curvature H^2 and to the Gaussian curvature K but the second one gives just a constant contribution to the total energy (due to Gauss-Bonnet theorem) and is irrelevant for our analysis. In the lowest-order (harmonic) approximation $H \propto \nabla^2 h$ and, thus, the bending energy has the form

$$\mathcal{H}_b = \frac{\kappa}{2} \int d^2\mathbf{r} (\nabla^2 h)^2, \quad (79)$$

In the harmonic approximation, the correlation function of the Fourier components of $h(\mathbf{r})$, $\langle |h_{\mathbf{q}}|^2 \rangle$ is calculated immediately:

$$\langle |h_{\mathbf{q}}|^2 \rangle = \frac{T}{\kappa q^4}. \quad (80)$$

Thus, the mean square amplitude of out-of-plane displacement is

$$\langle h^2 \rangle = \sum_{\mathbf{q}} \langle |h_{\mathbf{q}}|^2 \rangle \simeq \frac{T}{\kappa} L^2, \quad (81)$$

where L is the sample size and we have introduced a cutoff of divergent integral in Eq. (81) at $q_{\min} \simeq 1/L$. Thus, typical amplitude of out-of-plane fluctuations is proportional to the sample size. The correlation function of the Fourier components of the normal vectors,

$$G(q) = q^2 \langle |h_{\mathbf{q}}|^2 \rangle = \frac{T}{\kappa q^2} \quad (82)$$

is also singular at small wave vectors and, thus, the correlator $\langle \vec{n}(\vec{R}) \vec{n}(0) \rangle$ behaves logarithmically at $R \rightarrow \infty$ whereas for a flat membrane it should tend to a constant (normals are more or less parallel at large distances). As a result, the model with the Hamiltonian (79) describes not a flat but a *crumpled* membrane.

The higher-order terms in the expansion of the mean curvature H in ∇h renormalize the effective bending rigidity [132],

$$\kappa_{eff}(T) = \kappa - \frac{3T}{4\pi} \ln \frac{L}{a}, \quad (83)$$

thus, the membrane becomes less rigid as the temperature increases.

The situation is totally different for *crystalline* membranes where the coupling between out-of-plane (bending) $h(\mathbf{r})$ and in-plane $\mathbf{u}(\mathbf{r})$ atomic displacement becomes crucially important [128, 134]. It follows from the elasticity theory [120, 135] that the total elastic energy in this case is written as (cf. Eq. (62))

$$\mathcal{H} = \int d^2\mathbf{r} \left[\frac{\kappa}{2} (\nabla^2 h)^2 + \mu u_{\alpha\beta}^2 + \frac{\lambda}{2} u_{\alpha\alpha}^2 \right], \quad (84)$$

$u_{\alpha\beta}$ is given by Eq. (71) We keep there quadratic terms in the derivatives of out-of-plane deformation but not in the derivatives of in-plane deformations since the former are, at the average, much larger. The model described by the

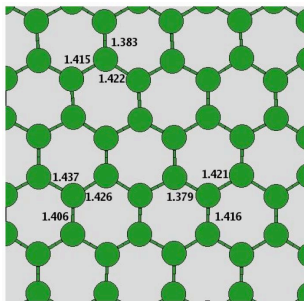


FIG. 11: Portion of one typical atomic configuration of graphene sample at room temperature. The numbers indicate the bond length in Å (taken with permission from Ref. [129]).

Hamiltonian (84) is essentially nonlinear. Since the Hamiltonian is quadratic in in-plane components of the distortion tensor, $\frac{\partial u_\alpha}{\partial x_\beta}$, the partition function can be integrated over the latter and the effective Hamiltonian for out-of-plane deformations only can be exactly derived [128, 134, 136, 137]:

$$\mathcal{H} = \int d^2\mathbf{r} \left[\frac{\kappa}{2} (\nabla^2 h)^2 + \frac{K_0}{8} \left(P_{\alpha\beta}^T \frac{\partial h}{\partial x_\alpha} \frac{\partial h}{\partial x_\beta} \right)^2 \right], \quad (85)$$

where $P_{\alpha\beta}^T = \delta_{\alpha\beta} - (\partial^2 / \partial x_\alpha \partial x_\beta) / \nabla^2$ is the operator separating transverse components and

$$K_0 = \frac{4\mu(\mu + \lambda)}{2\mu + \lambda} \quad (86)$$

The Hamiltonian (85) describes interactions of soft (long-wavelength) fluctuations, similar to the Ginzburg-Landau-Wilson Hamiltonian for the critical point [6, 7, 138]. The difference is that two-dimensional systems are “critical” at *any* finite temperatures. In analogy with the theory of critical phenomena, one can introduce [128, 134] scaling hypothesis for correlation functions and the corresponding exponents η, η', ζ related with the behavior of effective bending rigidity, $\kappa_{eff}(q) \propto q^{-\eta}$, elastic moduli, $\mu_{eff}(q), \lambda_{eff}(q) \propto q^{\eta'}$ and characteristic out-of-plane deformation, $\sqrt{\langle h \rangle^2} \propto L^\zeta$. All these exponent can be expressed through the only exponent η :

$$\zeta = 1 - \eta/2, \quad \eta' = 2(1 - \eta) \quad (87)$$

The normal-normal correlation function, instead of Eq.(82), behaves as

$$G(q) \propto q^{-(2-\eta)} \quad (88)$$

at $q \rightarrow 0$, and the membrane is “flat” (in a sense that $\langle \vec{n}(\vec{R}) \vec{n}(0) \rangle \rightarrow const$ at $R \rightarrow \infty$) for $0 < \eta < 1$. However, the amplitude of out-of-plane displacements grows with the sample size which means that the membrane is essentially corrugated, in contrast with the surface of three-dimensional crystals where $\sqrt{\langle h \rangle^2}$ remains much smaller than the interatomic distances. Note that the *in-plane* phonon modes become even softer due to the coupling with the out-of-plane ones, since $\mu_{eff}(q), \lambda_{eff}(q) \rightarrow 0$ at $q \rightarrow 0$. In this sense, there is no real crystalline order since there is no infinitely narrow delta-functional Bragg peaks but, instead, some power-law singularities at the reciprocal lattice points so the Mermin theorem is, of course, not violated. This broadening of the Bragg peaks is clearly seen both in experiments [43] and simulations [47] for graphene. The continuum model (84), which is called the model of phantom membranes, has a transition to a crumpled phase at a temperature of the order of κ . The term “phantom” means that the model does not include self-avoidance, the natural condition of true physical systems. It is assumed that self-avoidance removes the phase transition to the high temperature crumpled phase while the scaling properties of the “flat” phase remain the same as in phantom membranes [128]. To calculate the exponent η some approximations should be done. The ϵ -expansion in $\epsilon = 4 - d$, where d is the space dimensionality, so efficient in the theory of critical phenomena [6, 7, 138] is practically useless for low-dimensional systems. Instead, one can use an expansion in inverse number of component n of the vector of out-of-plane displacement h . Of course, in real physical problem $n = 1$. However, if one consider D -dimensional membrane in d -dimensional space, $n = d - D$ can be formally

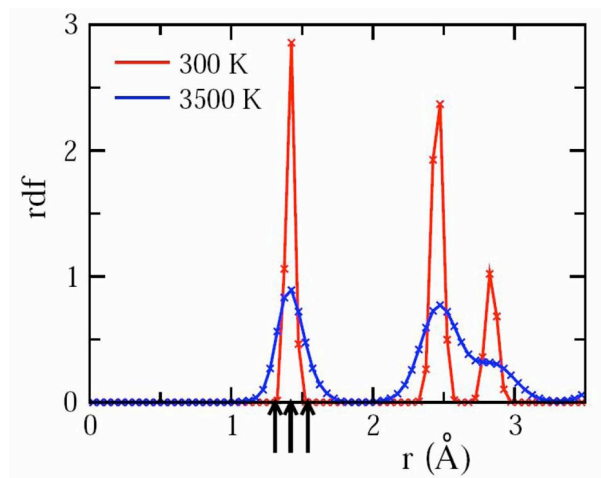


FIG. 12: Radial distribution function at $T = 300$ K and $T = 3,500$ K as a function of interatomic distance. The arrows indicate the length of double ($r = 1.31$ Å), conjugated ($r = 1.42$ Å) and single ($r = 1.54$ Å) bonds (taken with permission from Ref. [129]).

considered as a large parameter in the problem [134], than, $\eta \approx 1/n$. More subtle use of this parameter is the Self Consistent Screening Approximation [136, 137] which neglects vertex corrections when consider diagrammatically the interaction of fluctuations; the vertex corrections have formal smallness in $1/n$. This approximation (for the real case $d = 3, D = 2$) yields $\eta = 2(\sqrt{15} - 1)/7 \approx 0.821$. A very recent non-perturbative renormalization group approach [139] yields a close value $\eta \approx 0.849$. The discretized version of the model (84) was investigated by Bowick *et al.* [138] by means of Monte Carlo simulations giving $\eta \approx 0.72$.

For the case of crystalline membranes, contrary to the case of liquid ones, the effective bending rigidity grows with the temperature [128], due to anharmonic coupling of out-of-plane and in-plane displacements. This result has a very simple physical meaning: it is known from the elasticity theory that corrugations strengthen plates making them effectively thicker [120, 135], and amplitudes of corrugations increase with the temperature increase.

The long-range orientational (“hexatic”) or translational (crystalline) order can be in principle destroyed by spontaneous creation of topological defects, disclinations and dislocations, respectively. Whereas for two-dimensional crystals in two-dimensional space the disclination energy grows with the sample size as L^2 (and the dislocation one as $\ln L$) for the case under consideration (two-dimensional crystals in three-dimensional space) the elastic energy strongly decreases due to screening by bending deformations; as a result, the disclination energy grows as $\ln L$ and the dislocation energy remains constant in the thermodynamic limit $L \rightarrow \infty$ [128]. This means that, strictly speaking, the long-range crystalline order is destroyed also via the creation of dislocations by thermal fluctuations. However, for graphene with its extremely strong chemical bonding (e.g., vacancy formation energy about 7 eV [140]) the concentration of such thermal dislocations should be very small; no evidences of their formation were found in atomistic simulations for temperatures up to 3000 K [66, 129].

A quantitative information about intrinsic corrugations in graphene can be obtained using atomistic simulations with some interatomic interaction potential for carbon (of course, it cannot be just pairwise potential, it should be dependent on the angles between bonds which is crucially important for a covalent chemical bonding). The Monte Carlo simulations [66, 129, 133] used the so called bond-ordered potential LCBOPII [141]. This potential is based on a large database of experimental and theoretical data for molecules and solids and has been proved to describe very well thermodynamic and structural properties of all phases of carbon and its phase diagram in a wide range of temperatures and pressures [141, 142]. Of particular importance here, is that bond order potentials correlate coordination to bond strength, allowing changes between single, double and conjugated bonds with the correct energetics.

A typical configuration of graphene at room temperature obtained in the simulations is shown in Figure 10. For the crystallite of about 10000 atoms a typical size of the height fluctuations was 0.07 nm (a half of interatomic distance) with a typical spatial scale 5 to 10 nm. As a result, the bond lengths are rather broadly distributed, changing between lengths of double and single carbon-carbon bonds (Figs. 11 and 12). The normal-normal correlation function shown in Fig. 13 (Fig. 2 from [133]) demonstrates a crossover from the harmonic behavior (82) to anharmonic one, (88), at $q^* \approx 2 \text{ nm}^{-1}$, with $\eta \approx 0.85$. This value is in a very good agreement with the predictions of the continuum model [136, 139].

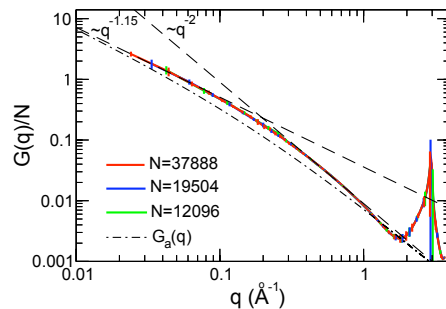


FIG. 13: Normal-normal correlation functions calculated for three systems with $N=12096$, 19504 , and $N=37888$ carbon atoms. The dashed lines show the asymptotic harmonic behavior with power laws with between these limiting cases (taken with permission from Ref. [133]).

V. OBSERVABLE CONSEQUENCES OF THE GAUGE FIELDS: MICROSCOPIC EFFECTS

A. Index theorems and zero energy states

The energy spectrum of massless Dirac fermions coupled to gauge fields has a very special property, the existence of zero-energy chiral modes equally shared by electrons and holes. This is a consequence of one of the most important theorems of modern mathematics, the Atiyah-Singer index theorem [143, 144]. This theorem has important applications in quantum field and superstring theories [145, 146]. It was mentioned already in one of the first works on graphene [14] (see also Ref. [17]) that the anomalous (“half-integer”) quantum Hall effect in single-layer graphene is a consequence of the Atiyah-Singer theorem (later [147] a similar statement has been also proven for the anomalous quantum Hall effect in graphene bilayer [148]). The existence of the zero-energy states for massless Dirac fermions in inhomogeneous magnetic fields in two dimensions was demonstrated explicitly long ago by Aharonov and Casher [149]. Here we present their result and discuss its relevance for graphene physics.

Let $\mathbf{A}(x, y)$ is an arbitrary two-dimensional vector potential satisfying the condition $\nabla \mathbf{A} = 0$. Thus, one can introduce a scalar “potential” $\phi(x, y)$ such that, that

$$A_x = -\partial_y \phi, A_y = \partial_x \phi \quad (89)$$

and

$$\nabla^2 \phi = B \quad (90)$$

is the magnetic field. For zero-energy the Dirac equation is split into two independent equations for the spinor components ψ_σ ($\sigma = \pm$)

$$(\partial_x + i\sigma\partial_y - iA_x + \sigma A_y) \psi_\sigma = 0 \quad (91)$$

The potential ϕ can be excluded by the substitution

$$\psi_\sigma = e^{-\sigma\phi} f_\sigma \quad (92)$$

where

$$(\partial_x + i\sigma\partial_y) f_\sigma = 0 \quad (93)$$

and, thus, f_+ and f_- are analytic and complex conjugated analytic entire functions of $z = x + iy$, respectively.

Since the Green’s function of the Laplace operator in two dimensions

$$\left\langle \mathbf{r} \left| \frac{1}{\nabla^2} \right| \mathbf{r}' \right\rangle = \frac{1}{2\pi} \ln \frac{|\mathbf{r} - \mathbf{r}'|}{r_0} \quad (94)$$

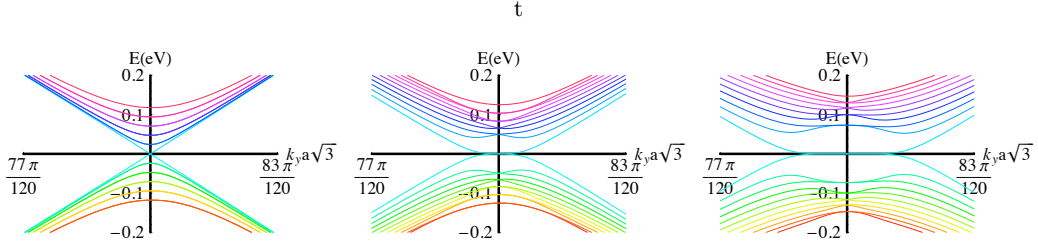


FIG. 14: Low energy states induced by a one dimensional ripple modelled by a sine modulation of the atomic displacements. The average hopping is $t_{\parallel} = 3\text{eV}$. The width of the ripple is $1200a = 168\text{nm}$. The modulations of the hoppings are: Left, $\delta t/t = 0$, center, $\delta t/t = 0.02$, right, $\delta t/t = 0.04$ (taken with permission from Ref. [152]).

the solution of Eq.(90) at large distances has the asymptotics), with

$$\phi(r) \simeq \frac{\Phi}{2\pi} \ln \frac{r}{r_0} \quad (95)$$

where $\Phi = \int dx dy B$ is the total magnetic flux through the system. Thus, at large r

$$e^{-\sigma\phi} \simeq \left(\frac{r_0}{r}\right)^{\sigma\Phi/2\pi} \quad (96)$$

Since the entire function cannot go to zero in all directions at infinity, ψ_{σ} can be normalizable only assuming that $\sigma\Phi > 0$, that is, zero-energy solutions can exist only for one (pseudo)spin directions, depending on the sign of the total magnetic flux.

Let us count how many independent solutions of Eq. (93) we have. As a basis, we can choose just polynoms searching the solutions of the form

$$\psi_{+} = z^j e^{-\phi} \quad (97)$$

(to be specific, we consider the case $\Phi > 0$, where $j = 0, 1, 2, \dots$. One can easily see from Eq.(96) that the solution is integrable with the square only assuming that $j \leq N$, where N is the integer part of $\Phi/2\pi$).

According to the Atiyah-Singer theorem, the index of Dirac operator in our situation, that is, the difference between numbers of solutions with zero energy and positive and negative sigmas is equal to N . The Aharonov-Casher procedure gives us an explicit shape of these solutions and proves that, actually, there are solutions only for one spin projection. These solutions are robust (topologically protected) in a sense that they are not shifted from zero energy of broadened by any inhomogeneities of the magnetic field.

It has been proven in Ref. [147] that the Atiyah-Singer theorem can be applied also for the case of bilayer graphene; in this situation the number of zero-energy solutions is twice the number of the solutions for single layer with the same magnetic flux. Explicitly, these solutions have been constructed, as a generalization of the Aharonov-Casher solutions, in Ref. [150]. Thus, the zero-energy states in the case of bilayer are also topologically protected and cannot be broadened by any inhomogeneities of the magnetic field.

This conclusion leads to an important consequence for the quantum Hall effect in single- and bilayer graphene. Whereas smooth inhomogeneities of electrostatic potential lead to a broadening of all Landau levels, like in conventional homogeneous two dimensional electron gas, and zero-energy Landau level is not an exception [27], random vector potential due to ripples cannot broaden the zero-energy Landau level which, thus, should be essentially narrower than the other Landau levels. This conclusion seems to be in an agreement with experimental data on quantum Hall activation gaps in single-layer graphene [151]. It would be very interesting to check it also for the case of bilayer. If the pseudomagnetic field created by ripples is strong enough it can result in the appearance of the mid-gap states [152]. Figure 14[152] shows energy spectrum of a graphene ribbon with the simplest one-dimensional sine modulation of the atomic displacements and, thus, vector potential. One can clearly see an appearance of the midgap states for strong enough modulation. If the modulated scalar potential is also present the Atiyah-Singer theorem is not applicable and, in general, a gap can open. General conditions for opening the gap in oscillating electric and magnetic fields are discussed in Ref.[153]. The existence of the midgap states for sine modulation has been confirmed by ab initio calculations [154].

The midgap states are probably essential in the chemistry of graphene. It was demonstrated by a straightforward ab initio calculation [155] that the energy of chemisorption of hydrogen on rippled graphene is much lower than that

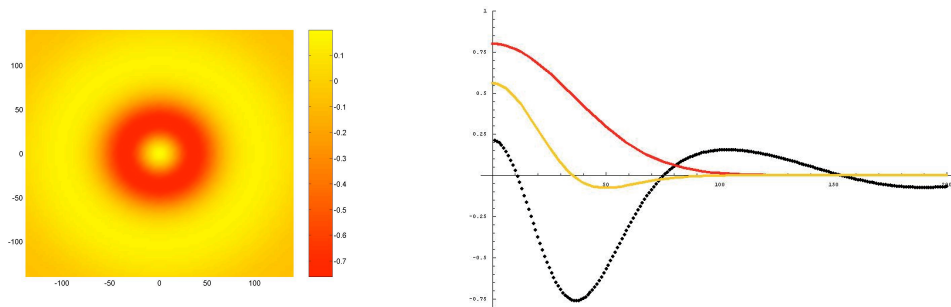


FIG. 15: (Color online) Left: Effect of the curved bump of fig. 6 on the local density of states of the graphene sheet. The color code is indicated in the figure. Darker (lighter) areas represent negative (positive) corrections to the density of states of the flat graphene sheet. Right: Correction to the density of states (dotted line) in arbitrary units, versus the shape of defect (red – upper – line) and curvature of the defect (yellow – middle – line) for a gaussian bump of an average width of 50 Å (taken with permission from Ref. [101]).

on the flat samples indicating that the ripples can be centers of chemical activity. This effect is especially strong if the corrugations are large enough to create the midgap states: hydrogen leads to the splitting of the peak at zero energy and thus to an essential total energy decrease. This splitting results from a resonance between the midgap states created by hydrogen itself and those created by the ripples.

B. Inhomogeneities in the electronic density

One of the effects of having samples locally curved or rippled is to induce charge inhomogeneities in the samples. This effects were studied within the geometric (covariant) approach in Refs. [50, 101] by computing the local density of states through the Green's function. In a curved surface, the spinor Green's function obeys the equation

$$i\gamma^\alpha e_\alpha^\mu (\partial_\mu - \Omega_\mu) G(\mathbf{r}, \mathbf{r}') = \delta(\mathbf{r} - \mathbf{r}')(-g)^{-\frac{1}{2}}, \quad (98)$$

where the geometric factors are described in Appendix A. From this equation the local density of states can be obtained through the expression:

$$\rho(E, \mathbf{r}) = -\frac{1}{\pi} \text{ImTr}[G(E, \mathbf{r}, \mathbf{r})\gamma^0]. \quad (99)$$

The gaussian shape of Fig. 6 was shown in [101] to induce oscillations in the density of states of the type depicted in Fig. 15 a). It is interesting to note that the local maximum of correction to the flat DOS corresponds to the regions in space where the curvature changes sign as it can be seen in Fig. 15 b). An interesting prediction of this model is a space variation of the Fermi velocity \tilde{v}_r in the radial direction given by

$$\tilde{v}_r(r, \theta) = \frac{v_F}{\sqrt{1 + \alpha f(r)}}, \quad (100)$$

where $f(r)$ is the equation of the surface (35). It is worth mentioning that irrespective of the shape of the corrugations, the effective Fermi velocity in the presence of intrinsic curvature will always be less than the flat value v_F .

The same formalism applied to a given distribution of topological defects gives rise also to inhomogeneities of the local DOS where a local charge density is accumulated around the pentagons and repelled near the heptagons [50].

C. Strains, gauge fields, and weak (anti)localization

In normal metals, the wavevector of the electrons at the Fermi energy is comparable to the lattice spacing. This allows us to define wavepackets which are much smaller than the distance over which the electrons move between collisions, the mean free path. The trajectories of these wavepackets in an applied electric field are described by the classical equations of motion.

A full analysis of the conductance of a metal requires the analysis of the effects associated to the wave nature of the electrons [156, 157]. These corrections to the classical description can be studied as a series in powers of

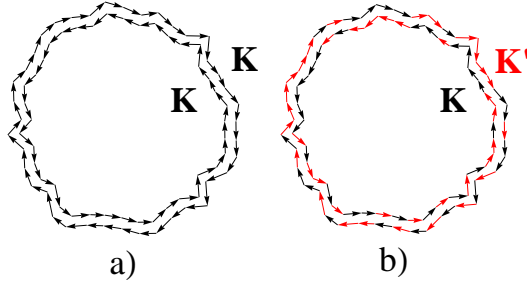


FIG. 16: (Color online) Counterpropagating paths which contribute to the magnetoresistance in weak magnetic fields. a) Paths where the wavefunctions belong to the same valley. Although these paths are not related by time reversal symmetry, near the Dirac point are sufficiently similar to lead to interference effects. b) Paths related by time reversal symmetry. Interference between such paths is the leading contribution to the magnetoresistance if intervalley scattering is sufficiently strong.

$k_F \ell$, where k_F is the inverse Fermi wavelength, and ℓ is the mean free path. The classical description is obtained in the limit $k_F \ell \rightarrow \infty$. The leading quantum effects arise from the interference between two counterpropagating paths, as schematically depicted in Fig. 16. In a normal metal, such paths show a constructive interference. As a result, the probability that the electron is scattered backwards is enhanced with respect to the classical case. This interference is suppressed in the presence of a magnetic field, and this leads to an increase of the conductivity in weak magnetic fields, the so called weak localization effect. When $k_F \ell \rightarrow 1$, interference effects become strong, and they lead to the formation of localized wavefunctions[158, 159], and to insulating behavior. In systems with large spin-orbit coupling, the spin is pinned to the momentum the electron. The rotation of the spin when the electron moves around a closed loop adds a phase of π to the wavefunction. As a result, closed loops show negative interference, and the magnetoresistance is negative, the so called weak antilocalization.

Electrons in graphene have the sublattice and the valley degrees of freedom, which can play a role similar to the spin in systems with a strong spin-orbit coupling. The situation is schematically shown in Fig. 16. Counterpropagating paths can exist where the electron resides always in the same valley, as shown in Fig. 16 a). The two paths are not exactly the same, because they are not related by time reversal symmetry, which exchanges the valleys. The equivalence between the two paths arising from the same valley becomes exact at the Dirac point. As a result, these paths can contribute to the magnetoresistance for weak magnetic fields, provided that intervalley scattering can be neglected. The contribution of these paths leads to weak antilocalization, because of the contribution to the total phase of the sublattice polarization, the pseudospin. This situation can be also described as the result of the existence of an approximate symmetry which plays the role of time reversal symmetry within each valley.

The contribution of the paths in Fig. 16 a) is suppressed by the gauge fields due to lattice deformations [41, 42]. The interference between these paths is also reduced by the inequivalence of the wavefunctions from the same valley with opposite momenta, which increases away from the Dirac energy, the so called trigonal warping [160]. As a result, there is a regime in graphene, when intervalley scattering is small, but gauge fields are significant, where there are neither weak localization nor weak antilocalization effects. This regime describes well the experimental situation [41, 161]. The absence of any magnetoresistance in the most recent experiments [161] is remarkable, because the intravalley scattering length associated with gauge fields or other perturbations which break the effective time reversal symmetry at each valley is much shorter than other scales, and it is difficult to explain by the height of the ripples observed by AFM measurements.

In the presence of strong intravalley scattering, the leading paths which contribute to the quantum corrections of the conductivity are shown in Fig. 16 b). These are the same processes which describe the magnetoresistance in ordinary metals, and they lead to weak localization, and a negative magnetoresistance. Bilayer graphene, were smaller corrugations are expected, shows weak localization effects at low fields [162].

D. Modelling disorder in graphene with random gauge fields

The influence of ripples and other types of disorder on the transport properties of a system requires to assume a density of defects with some statistical distribution and to average over defects. The standard techniques of disordered electrons [163] can be applied to rippled graphene by averaging over the random effective gauge fields induced by curvature or elastic deformations. Modelling disorder with random magnetic fields was first proposed in the context of disordered degenerate semiconductors [164, 165]. Dirac fermions in random magnetic fields were used to study critical point transitions between integer and fractional fillings in the Quantum Hall Effect [166, 167]. Most of these works involved disordered systems without interactions what reduces effectively the dimensionality of the problem to two dimensions allowing the use of very powerful tools as bosonization or conformal field theory techniques [168]. A complete classification of disordered graphene without interaction in the random matrices language was worked out in [169–171]. Combined disorder and interactions was first addressed in the context of critical points between integer and fractional fillings in the Quantum Hall Effect [166, 167, 172] and later applied to the graphene problem in [173–175]. A recent complete survey can be found in [176] and the included references. A computation of the effect of the curvature induced by topological defects on the conductivity of neutral graphene using the random field approach was done in [103].

The low energy excitations in graphene combining the two Dirac points can be described by the four-dimensional Hamiltonian:

$$H_0 = iv_F \int d^2x \bar{\Psi}(\vec{x}) \vec{\gamma} \cdot \vec{\nabla} \Psi(\vec{x}) \quad (101)$$

where $\bar{\Psi} \equiv \Psi^\dagger \gamma_0$ with the 4×4 matrix $\gamma_0 \equiv \sigma_3 \otimes \sigma_3$ (in this section we put $\hbar = 1$). We further have $\vec{\gamma} \equiv (\gamma_1, \gamma_2) = (-i\sigma_2, i\sigma_1) \otimes \sigma_3$. The σ_μ denote the usual Pauli matrices such that $\{\gamma_\mu, \gamma_\nu\} = 2g_{\mu,\nu} \mathbf{1}_{4 \times 4}$, $g_{\mu,\nu}$ denoting the Minkowski tensor where $g_{0,0} = 1$, $g_{i,i} = -1$ with $i = 1, 2$, and zero otherwise.

The long range Coulomb interaction in terms of the Dirac spinors reads

$$H_{ee} = \frac{v_F}{4\pi} \int d^2x d^2x' \bar{\Psi}(\vec{x}) \gamma_0 \Psi(\vec{x}) \frac{g}{|\vec{x} - \vec{x}'|} \bar{\Psi}(\vec{x}') \gamma_0 \Psi(\vec{x}') \quad (102)$$

where $g = e^2/v_F$ is the dimensionless coupling constant.

In order to describe disorder effects, the Dirac spinors are coupled to a gauge field $A(\vec{x})$,

$$H_{disorder} = \frac{v_\Gamma}{4} \int d^2x \bar{\Psi}(\vec{x}) \Gamma \Psi(\vec{x}) A(\vec{x}) \quad (103)$$

where v_Γ characterizes the strength and the 4×4 matrix Γ the type of the vertex. In general, $A(\vec{x})$ is a quenched, Gaussian variable with the dimensionless variance Δ , i.e.,

$$\langle A(\vec{x}) \rangle = 0 \quad , \quad \langle A(\vec{x}) A(\vec{x}') \rangle = \Delta \Gamma \delta^2(\vec{x} - \vec{x}') \quad . \quad (104)$$

Inclusion of long ranged correlated disorder is a much more difficult task that has been addressed in [103, 177, 178].

A perturbative renormalization group (RG) approach to the problem as the one performed in [174–176] allows to study the phase diagram of the system as a function of the Coulomb interaction parameter and the strength of the various disorder couplings. It is known that the (unscreened) Coulomb interactions in graphene induce an upward flow of the Fermi velocity that grows at low energies [23, 179]. That makes the effective coupling $g \sim \frac{e^2}{v_F}$ to flow to zero. Typically the inclusion of disorder changes the flow of the Fermi velocity due to wave function renormalization, i.e., $Z_{v_F} \rightarrow Z_{v_F}/Z_\Psi$. In the simplest one loop analysis done in [174], from the β -function $\beta_{v_F} = \Lambda \partial_\Lambda Z_{v_F} \tilde{v}_F$, one obtains flow equations for the effective Fermi velocity v_F^{eff} of the form:

$$\frac{d}{d\ell} \frac{v_F^{eff}}{\tilde{v}_F} = \frac{1}{16\pi} \left[\frac{e^2}{v_F^{eff}} - \frac{\Delta}{2} \left(\frac{v_\Gamma^{eff}}{v_F^{eff}} \right)^2 \right], \quad (105)$$

where $\ell = \ln \Lambda/\Lambda_0 \sim 1/\varepsilon$.

The phase diagrams obtained in [174] for the various types of disorder considered can be summarized as follows:

i) For a random chemical potential ($\Gamma = \gamma_0$), $v_\Gamma = v_1$ remains constant under renormalization group transformation. There is an unstable fixed line at $v_F^* = v_1^2 \Delta / (2e^2)$. In the (g, Δ) -plane, the strong-coupling and the weak-coupling phases are separated by a hyperbola, with the critical electron interaction $g^* = e^2/v_F^* = 2e^4/(v_1^2 \Delta)$.

ii) A random gauge potential involves the vertices $\Gamma = i\gamma_1, i\gamma_2$. The vertex strength renormalizes as $v_\Gamma = v_F$. There is an attractive Luttinger-like fixed point for each disorder correlation strength Δ given by $v_F^* = 2e^2/\Delta$ or $g^* = \Delta/2$.

iii) For a random mass term $\Gamma = \mathbf{1}_{4 \times 4}$, topological disorder $\Gamma = i\gamma_5$, and $\Gamma = i\tilde{\gamma}_5$, we have $v_\Gamma = v_F^2/v_3$. There is thus again an attractive Luttinger-like fixed point for each disorder correlation strength Δ given by $v_F^* = \sqrt[3]{2v_3^2 e^2/\Delta}$ or $g^* = \sqrt[3]{\Delta e^4/(2v_3^2)}$.

More sophisticated calculations do not introduce essential changes in this simple description.

E. Scattering of charge carriers by gauge fields

High electron mobility found already in the first work on graphene [13] is one of its most attractive features, in view of potential applications. Submicron mean free path is routinely achievable; even order of magnitude higher mobility $\mu \simeq 10^5 \text{ cm}^2/\text{Vs}$ was reached recently for freely suspended graphene membranes [180, 181]. Despite numerous experimental and theoretical efforts, the physics of this high mobility is not well understood yet and there are still controversial views on the main mechanism limiting the electron mobility. Following a general line of our review, we discuss here the role of gauge fields created by corrugations of graphene in its electron transport properties.

We proceed with a simple and physically transparent semiclassical picture based on the Boltzmann kinetic equation. Its applicability to graphene is not a priori obvious, due to potential role of quantum relativistic effects known as the Zitterbewegung (in terms of solid state physics - interband processes mixing electrons and holes) [182, 183]. However, it has been formally demonstrated in Ref. [183], using short-range scatterers as an example, that the interband scattering processes are negligible, and, thus, the semiclassical Boltzmann equation is justified, assuming that

$$\varepsilon_F \tau / \hbar \gg 1 / |\ln(k_F a)|, \quad (106)$$

where ε_F and k_F are the Fermi energy (counted from the Dirac point) and wave vector, respectively, and τ is the electron mean free path related with the resistivity ρ by the Drude formula [184]

$$\rho = \frac{2}{e^2 v_F^2 N(\varepsilon_F)} \frac{1}{\tau(k_F)}. \quad (107)$$

The condition (106) excludes only a relatively small doping interval where the conductivity is close to a minimal metallic conductivity of order of e^2/h . The expression for τ depends on the scattering mechanism. For point defects with the concentration n_{imp} and angular dependent scattering cross section $\sigma(\theta)$ one has [184, 185]

$$\frac{1}{\tau(k)} = n_{imp} v_F \sigma_{tr}(k), \quad (108)$$

where

$$\sigma_{tr} = \int_0^{2\pi} d\theta \frac{d\sigma(\theta)}{d\theta} (1 - \cos \theta), \quad (109)$$

is the transport cross section.

For the case of radially symmetric potential the scattering cross section can be expressed in terms of the scattering phases δ_m as [27, 28, 169, 186–190]

$$\sigma_{tr} = \frac{4}{k} \sum_{m=0}^{\infty} \sin^2(\delta_m - \delta_{m+1}). \quad (110)$$

Consider first the case of short-range scatterers with the radius of potential R much smaller than the electron de Broglie wavelength $\lambda_F = 2\pi/k_F$. Then only s -scattering survives ($m = 0$), with $\delta_0(k) \sim kR$ in a generic case, with a negligible contribution to the resistivity,

$$\rho \simeq \frac{h}{4e^2} n_{imp} R^2 \quad (111)$$

(we keep here and further a factor 4 to remind that there are four channels of conductivity, due to two valleys and two spin projections). This is not surprising: the massless Dirac fermions in graphene has the same dispersion law as light and, thus, obstacles with sizes smaller than the wavelength are inefficient, like in optics [191]. On the contrary, for conventional nonrelativistic two-dimensional electrons even weak scattering leads to a formation of shallow bound states and to singularities in the scattering matrix [192], namely, $\delta_0(k) \sim 1/\ln(kR)$. For the case of graphene, such situation takes place for a special case of “unitary”, or “resonant” scatterers with a quasibound state located near the Dirac point [27, 169, 186]. In such a case, the contribution to the resistivity is much stronger than (111) [27, 193, 194],

$$\rho \simeq \frac{h}{4e^2} \frac{n_{imp}}{n \ln^2(k_F R)} \quad (112)$$

where n is the charge carrier concentration.

For the case of long-range Coulomb scattering potential, the scattering phases are energy independent [187, 189, 195] which leads to a contribution to the resistivity inversely proportional to n ; taking into account the screening does not change this result [177, 196, 197]. A rough estimation for the resistivity reads [197]

$$\rho \simeq 20 \frac{h}{e^2} \frac{n_{imp}}{n} \quad (113)$$

Experimentally [14, 15], the resistivity is roughly inversely proportional to the charge carrier concentration, or, equivalently, the mobility is independent, or weakly dependent on n . Since the scattering by Coulomb charges is the simplest mechanism explaining this behavior it is not surprising that this was considered as an explanation “by default”. This explanation seems to be in agreement with experimental data on graphene chemically doped by potassium [198]. On the contrary, experiments on the chemical doping by gaseous impurities such as NO₂ show a rather weak dependence of the mobility on charge carrier concentration [199]. Recently, it was demonstrated that the mobility is also weakly sensitive to dielectric constant κ of substrate or to coverage of graphene by polar liquids with high κ , such as ethanol or water [200]. Clusterization of the charge impurities due to low diffusion barriers may be a possible explanation of their relatively small contribution to the resistivity [201, 202]. Anyway, the experimental data [200] probably mean that charge impurities cannot be the main factor limiting electron mobility in graphene.

Resonant scatterers such as vacancies [193] or covalently bond impurities [202, 203] might be another option. However, vacancies in graphene have huge energy, about 7 eV, and should be rather exotic (if not created intentionally as in experiments [204]); as for the covalent impurities it is not clear why they should *always* have resonant levels close to the Dirac point. For these reasons, an alternative scenario [194], the scattering by gauge fields created by frozen ripples, is worth to be considered seriously.

Let us consider a generic perturbation of the form

$$H' = \sum_{\mathbf{p}\mathbf{p}'} \Psi_{\mathbf{p}}^\dagger V_{\mathbf{p}\mathbf{p}'} \Psi_{\mathbf{p}'}, \quad (114)$$

where $\Psi_{\mathbf{p}}$ is the Dirac spinor dependent on quasimomentum \mathbf{p} and

$$V_{\mathbf{p}\mathbf{p}'} = V_{\mathbf{p}\mathbf{p}'}^{(0)} + A_{\mathbf{p}\mathbf{p}'}^{(x)} \sigma_x + A_{\mathbf{p}\mathbf{p}'}^{(y)} \sigma_y \quad (115)$$

contains both scalar (electrostatic) and vector (gauge field) random potentials. Following Ref. [194] we will use Born approximation in the perturbation H' and Kubo-Nakano-Mori approach [205–207] (as a recent example illustrating technical details see, e.g., Ref. [208]). This approach allows us to obtain, in a simple and straightforward way, the results which are equivalent to solution of Boltzmann equation by variational principle [184]. The inverse mean free path time is given by

$$\frac{1}{\tau} = \frac{1}{\hbar^2 \langle j_x^2 \rangle} \int_{-\infty}^{\infty} dt \langle [j_x(t), H'(t)] [H', j_x] \rangle, \quad (116)$$

where j_x is the current operator in x direction. Use of this approach in graphene should be done carefully, namely, only intraband (electron-electron or hole-hole, depending on the positions of the Fermi energy) contributions to the operators j_x and H' should be taken into account. An accurate justification of such procedure is done in Ref. [183]. For the case of static disorder, the result takes the form

$$\frac{1}{\tau} = \frac{4\pi}{\hbar N(\varepsilon_F)} \sum_{\mathbf{p}\mathbf{p}'} \delta(\varepsilon_{\mathbf{p}} - \varepsilon_F) \delta(\varepsilon_{\mathbf{p}'} - \varepsilon_F) (\cos \theta_{\mathbf{p}} - \cos \theta_{\mathbf{p}'})^2 |W_{\mathbf{p}\mathbf{p}'}|^2, \quad (117)$$

where $\theta_{\mathbf{p}}$ is the polar angle of the vector \mathbf{p} and

$$W_{\mathbf{p}\mathbf{p}'} = V_{\mathbf{p}\mathbf{p}'}^{(0)} \frac{1 + \exp[-i(\theta_{\mathbf{p}} - \theta_{\mathbf{p}'})]}{2} + \frac{1}{2} \left[\left(A_{\mathbf{p}\mathbf{p}'}^{(x)} + iA_{\mathbf{p}\mathbf{p}'}^{(y)} \right) \exp(-i\theta_{\mathbf{p}}) + \left(A_{\mathbf{p}\mathbf{p}'}^{(x)} - iA_{\mathbf{p}\mathbf{p}'}^{(y)} \right) \exp(i\theta_{\mathbf{p}'}) \right]. \quad (118)$$

Note that the electrostatic part of the scattering disappears for the back scattering ($\theta_{\mathbf{p}} - \theta_{\mathbf{p}'} = \pi$) which is related to the ‘‘Klein tunneling’’[25] but this is not the case for the scattering by vector potential. For a rough estimations in order of magnitude Eq. (117) can be rewritten as

$$\frac{1}{\tau} \simeq \frac{2\pi N(\varepsilon_F)}{\hbar} \left(\left\langle V_{\mathbf{q}}^{(0)} V_{-\mathbf{q}}^{(0)} \right\rangle + \left\langle \mathbf{A}_{\mathbf{q}} \mathbf{A}_{-\mathbf{q}} \right\rangle \right)_{q \approx k_F}, \quad (119)$$

where $\mathbf{q} = \mathbf{p}' - \mathbf{p}$ is the scattering vector. Since $N(\varepsilon_F) \propto k_F$, to have concentration independent mobility one needs that one of the correlation functions in Eq. (119) scales as $1/q^2$. Note that the second term, that is, the scattering by gauge fields, is not sensitive to dielectric screening.

Consider now the case of scattering by gauge fields created by intrinsic ripples due to thermal fluctuations (see Section IV D). For not too small wave vectors, in the harmonic regime, $q > q^*$ one can neglect a coupling between bending and stretching modes. This case is relevant for electron transport assuming that

$$k_F > q^*, \quad (120)$$

which does not look too restrictive. Further we will assume this condition to be satisfied. Thus, the vector potential is quadratic in derivatives $\partial h/\partial x, \partial h/\partial y$ and the estimation of the correlation function in (119) is

$$\left\langle \mathbf{A}_{\mathbf{q}} \mathbf{A}_{-\mathbf{q}} \right\rangle \approx \left(\frac{\hbar v_F}{a} \right)^2 \sum_{\mathbf{q}_1 \mathbf{q}_2} \langle h_{\mathbf{q}-\mathbf{q}_1} h_{\mathbf{q}_1} h_{-\mathbf{q}+\mathbf{q}_2} h_{-\mathbf{q}_2} \rangle [(\mathbf{q} - \mathbf{q}_1) \cdot \mathbf{q}_1] [(\mathbf{q} - \mathbf{q}_2) \cdot \mathbf{q}_2], \quad (121)$$

and the correlator in right-hand side of Eq. (121) can be decoupled by Wick theorem since the field $h(x, y)$ can be considered as a Gaussian in this regime. Thus, the scattering rate under the condition (120) is determined by the correlation function $\langle h_{\mathbf{q}} h_{-\mathbf{q}} \rangle$, that is, a Fourier component of the correlator

$$\Gamma(r) = \left\langle [h(r) - h(0)]^2 \right\rangle. \quad (122)$$

For thermally excited ripples in the harmonic regime

$$\Gamma(r) \simeq \frac{T}{\kappa} r^2, \quad (123)$$

which is a Fourier transformation of the Eq. (82). However, we consider first a more general case $\Gamma(r) \propto r^{2H}$ (for instance, for the ripples due to roughness of substrate one could expect $H \approx 1/2$, see Ref. [45]).

For $2H < 1$, the correlation function (121) has a finite limit at $q = 0$

$$\left\langle \mathbf{A}_{\mathbf{q}} \mathbf{A}_{-\mathbf{q}} \right\rangle_{q=0} \approx \left(\frac{\hbar v_F}{a} \right)^2 \frac{z^4}{R^2}, \quad (124)$$

where z and R are the characteristic height and radius of the ripples, respectively. The corresponding contribution to the resistivity is

$$\delta\rho \simeq \frac{h}{4e^2} \frac{z^4}{R^2 a^2}. \quad (125)$$

For $2 > 2H > 1$, the resistivity is proportional to n^{1-2H} and, for $2H = 1$, to $|\ln(k_F a)|$. In all these cases the corresponding contributions are too small in comparison with experimentally observed resistivity of graphene.

Let us now come back to the case of thermally excited ripples (123), $H = 1$. The integral in Eq. (121) is logarithmically divergent at small wave vectors, but this divergence should be cut at $q_1 \simeq q^*$. The corresponding contribution to the resistivity is estimated as

$$\delta\rho \simeq \frac{h}{4e^2} \left(\frac{T}{\kappa a} \right)^2 \frac{|\ln(q^* a)|}{n}. \quad (126)$$

This contribution gives us correct concentration dependence of the resistivity and, for room temperature $T = 300K$, correct order of magnitude of mobility, $\mu \simeq 10^4 \text{ cm}^2/\text{Vs}$. However, it predicts a strong temperature dependence of the resistivity, whereas experimentally it is very weak for the case of graphene at substrate [209]. The authors of Ref. [194] postulated that the ripple structure for graphene on substrate is frozen and becomes temperature independent below the room temperature.

The status of this hypothesis is not clear yet, neither theoretically nor experimentally. Whereas earlier STM studies of the ripples of graphene on substrate [45, 46] have found corrugations more or less similar to those of the substrate, recent work [210] claims that an “intrinsic” component postulated in Ref.[194] is also noticeable. Further investigations of the temperature dependence of the ripple structure are desirable to clarify the issue. From the theoretical point of view, it was demonstrated in Ref. [155] that ripples can attract adatoms and chemical groups (such as hydrogen or hydroxyl) and can be stabilized by them. Again, the problem requires more studies to clarify the situation.

Up to now, we consider out-of-plane deformations as a classical static field. In terms of quantum mechanics, the corresponding scattering mechanism is described as the two-phonon scattering processes by flexural phonons [209]. Introducing in a standard way [184] phonon creation and annihilation operators $b_{\mathbf{q}}^\dagger, b_{\mathbf{q}}$ one can represent the out-of-plane displacement field as

$$h(\mathbf{r}) = \sum_{\mathbf{q}} \sqrt{\frac{\hbar}{2M\omega_{\mathbf{q}}}} (b_{-\mathbf{q}}^\dagger + b_{\mathbf{q}}) e^{i\mathbf{q}\mathbf{r}}, \quad (127)$$

where M is the mass of carbon atoms, $\omega_{\mathbf{q}} = \sqrt{\kappa/\rho_m}q^2$ is the frequency of flexural phonons, ρ_m is the mass density. Since the vector potential is quadratic in $\partial h/\partial x, \partial h/\partial y$ the interaction Hamiltonian has the form

$$H' = \sum_{\mathbf{p}\mathbf{q}\mathbf{k}} \mathcal{A}_{\mathbf{p}\mathbf{q}\mathbf{k}} c_{\mathbf{p}}^\dagger c_{\mathbf{p}+\mathbf{k}-\mathbf{q}} (b_{-\mathbf{q}}^\dagger + b_{\mathbf{q}}) (b_{\mathbf{k}}^\dagger + b_{-\mathbf{k}}), \quad (128)$$

where we take into account only intraband scattering processes ($c_{\mathbf{p}}^\dagger, c_{\mathbf{p}}$ are electron creation and annihilation operators) and the amplitude \mathcal{A} behaves at small wave vectors as

$$\mathcal{A}_{\mathbf{p}\mathbf{q}\mathbf{k}} \propto \frac{\hbar v_F}{Ma\sqrt{\omega_{\mathbf{q}}\omega_{\mathbf{k}}}} \mathbf{q}\mathbf{k}. \quad (129)$$

Then, we simply substitute the Hamiltonian (128) into Eq. (109). The calculations are very similar to those for two-magnon scattering processes in half-metallic ferromagnets [208]. The result (where we skip for simplicity numerical factors of order one) reads

$$\begin{aligned} \frac{1}{\tau} \simeq & \frac{\hbar}{T(v_F M)^2 N(\varepsilon_F)} \sum_{\mathbf{p}\mathbf{p}'\mathbf{q}} \frac{(\mathbf{v}_{\mathbf{p}} - \mathbf{v}_{\mathbf{p}'})^2}{\omega_{\mathbf{q}}\omega_{\mathbf{q}+\mathbf{p}-\mathbf{p}'}} |\mathbf{q}(\mathbf{q} + \mathbf{p} - \mathbf{p}')|^2 f_{\mathbf{p}}(1 - f_{\mathbf{p}'}) \times \\ & \times [2N_{\mathbf{q}}(1 + N_{\mathbf{q}+\mathbf{p}-\mathbf{p}'}) \delta(\varepsilon_{\mathbf{p}'} - \varepsilon_{\mathbf{p}} - \hbar\omega_{\mathbf{q}} + \hbar\omega_{\mathbf{q}+\mathbf{p}-\mathbf{p}'}) + \\ & + (1 + N_{\mathbf{q}})(1 + N_{\mathbf{q}+\mathbf{p}-\mathbf{p}'}) \delta(\varepsilon_{\mathbf{p}'} - \varepsilon_{\mathbf{p}} + \hbar\omega_{\mathbf{q}} + \hbar\omega_{\mathbf{q}+\mathbf{p}-\mathbf{p}'}) + \\ & + N_{\mathbf{q}}N_{\mathbf{q}+\mathbf{p}-\mathbf{p}'} \delta(\varepsilon_{\mathbf{p}'} - \varepsilon_{\mathbf{p}} - \hbar\omega_{\mathbf{q}} - \hbar\omega_{\mathbf{q}+\mathbf{p}-\mathbf{p}'})], \end{aligned} \quad (130)$$

where $f_{\mathbf{p}} = f(\varepsilon_{\mathbf{p}})$ and $N_{\mathbf{q}} = N_B(\omega_{\mathbf{q}})$ are the Fermi and Bose distribution functions, respectively. For temperatures $T > \hbar\omega_{2k_F}^2 \simeq 1 \text{ K}$ phonons can be considered as classical neglecting the phonon frequencies in the conservation laws and replacing $N_{\mathbf{q}}$ by $T/\hbar\omega_{\mathbf{q}}$ in Eq. (130). Then, the result coincides with Eqs. (119), (126). The case of very low temperatures was considered in Ref. [211]. The minimal conductivity from a geometric model of topological lattice defects has been computed in [103].

VI. OBSERVABLE CONSEQUENCES OF THE GAUGE FIELDS: MESOSCOPIC EFFECTS, STRAINS IN SUSPENDED SAMPLES

A. Aharonov-Bohm phases in suspended samples

Mesoscopic deformations have been observed in graphene, and they can be induced in a controlled way. A particularly appropriate setup is a suspended graphene flake [43, 45, 180, 181, 212–219]. These systems are being very actively investigated, as the carrier mobility can be substantially larger than that of graphene on a substrate. The conductance minimum at the charge neutrality point is also sharper than in non-suspended samples. It has been

observed that these samples are under tension, which can be modulated by the electric force between the flake and the gate.

Typical sizes, L , of suspended samples are of the order of a few microns. Away from very close to the neutrality point these dimensions are much larger than the Fermi wavelength and the screening length, which is proportional to it. Hence, the long wavelength scalar potentials, $V_0(\vec{r})$, which may be generated by compression [62, 63] are screened. A simple Thomas-Fermi approximation leads to $V_{scr}(\vec{r}) \approx V_0(\vec{r})/(k_{FT}L)$ where $k_{FT} = e^2k_F/(\pi v_F)$ is the screening length. Gauge fields, on the other hand, remain unscreened.

1. Electronic transport in ballistic samples

We first assume that the samples are free of disorder and the only source of electron scattering is the gauge fields induced by the deformations. The simplest geometry which can be studied is a rectangular flake, as sketched in Fig. 7. If the bending energy is neglected, a complete analytical form can be found for the deformation[121]:

$$\begin{aligned} h(x) &= \frac{h_0}{L^2} \left(x^2 - \frac{L^2}{4} \right) \\ h_0^3 &= \frac{3\pi e^2}{64 E} (nL^2)^2 \end{aligned} \quad (131)$$

where $E = 4(\lambda + \mu)\mu/(\lambda + 2\mu) \approx 24 \text{ eV } \text{\AA}^{-2}$ is the Young's modulus of graphene. The in-plane stresses are:

$$u_x(x) = -\frac{2x^3 h_0^2}{3L^4} + \frac{x h_0^2}{6L^2} \quad (132)$$

where the boundary condition $u_x(\pm L/2) = 0$ has been used. As a result, the only non zero component of the strain tensor is:

$$u_{xx} = \frac{h_0^2}{6L^2} \quad (133)$$

The effect of the uniform strain is to induce a constant gauge field in the suspended region, $A_y = \beta u_{xx}/a$. The effect of this field is to shift the momentum parallel to the interface between the suspended and clamped region, k_y . An electron outside the suspended region with momentum $\vec{k} = (k_x, k_y)$ and energy $\epsilon_{\vec{k}} = v_F \sqrt{k_x^2 + k_y^2}$ can be either reflected at the boundary, with momentum $\vec{k}' = (-k_x, k_y)$ or transmitted, with momentum $\vec{k}'' = (k'_x, k_y + A_y)$ with k'_x such that $k'^2_x + (k_y + A_y)^2 = k_x^2 + k_y^2$. For incident momenta in the range $k_x^2 < 2A_y k_y + A_y^2$ there are no transmitted states, and the incident electron is reflected. The transmission amplitude, T , is determined by the equations:

$$\begin{aligned} 1 - R &= T \\ \frac{k_x + ik_y}{k} + \frac{-k_x + ik_y}{k} R &= \frac{k'_x + i(k_y + A_y)}{k} T \end{aligned} \quad (134)$$

and the transmission coefficient is $\mathcal{T} = |T|^2 (k'_x/k_x)$. At normal incidence, $k_y = 0$, the transmission coefficient can be expanded, $\mathcal{T} \approx 1 - A_y^2/(4k_x^2)$. The full expression for the transmission coefficient in the setup shown in Fig. 7, with two boundaries, can be obtained analytically [121]. The presence of two barriers leads to Fabry-Perot interferences as function of the incident angle, $\theta = \arctan(k_y/k_x)$. The angular dependence of the transmission is shown in Fig. 8. Note the skew scattering in the two valleys.

The above analysis is only valid for clean, ballistic systems. A finite concentration of impurities breaks the conservation of parallel momentum, which leads to the suppression of the transmission through each interface, Eq. (134). The lack of momentum conservation gives a finite transmission when strains in a ballistic sample completely suppresses it [121]. Evanescent waves allow carriers to penetrate in the suspended region. These carriers can be scattered into propagating modes by the impurities. A perturbative calculation shows that the induced transmission grows linearly with the concentration of impurities. The effect is proportional to the scattering strength, which can be parametrized in terms of the mean free path induced by the impurities.

B. Interferences between strains and real magnetic fields

The gauge fields associated to strains interfere with real magnetic fields applied to the system. When the strain can be treated as a small perturbation, the resulting effect is the existence of an inhomogeneous effective field distribution,

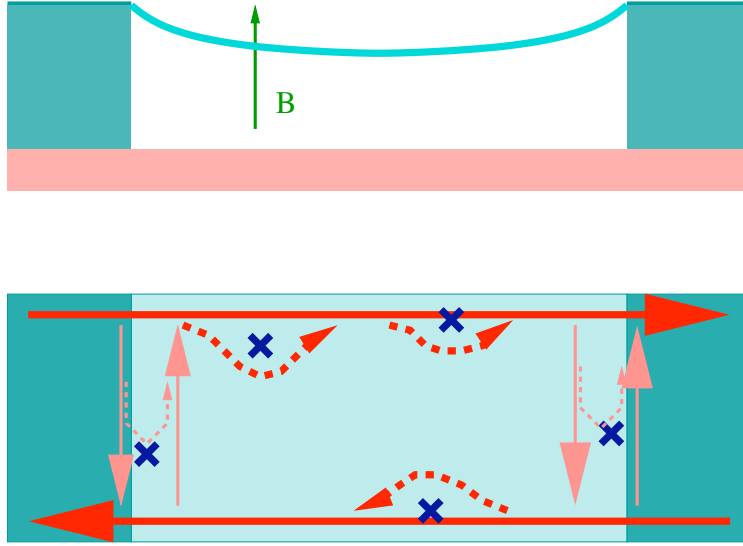


FIG. 17: Sketch of the expected effect in the presence of strains and a constant magnetic field. The geometry is the same as in Fig.[7]. The strains induce currents which lead to backscattering between the chiral edge states. A small concentration of impurities suppresses the effect.

given by the sum of the constant applied field and the effective field induced by the strains. Electronic states in the vicinity of the inhomogeneities are deformed, and can lead to localized “snake states”, where current flows along the perturbed region, as in the presence of a nonuniform magnetic field [220–222].

The qualitative effect of strains in the geometry in Fig. 7 is shown in Fig. 17. The strains induce currents parallel to the interface between the suspended and the non suspended regions, which allow for backscattering between the chiral edge states created by the magnetic field [223]. The states along the interface are not chiral, and impurities induce backscattering between them. If this effect is sufficiently strong, these states will become localized, and the coupling between the chiral edge channels will be suppressed.

The hamiltonian which describes the system, in the absence of impurities, and neglecting the edges, is:

$$\mathcal{H} = v_F \begin{pmatrix} 0 & i\partial_x + ik_y \mp iA_y^{strain}\theta(x) - i\frac{x}{l_B^2} \\ i\partial_x - ik_y \pm iA_y^{strain}\theta(x) + i\frac{x}{l_B^2} & 0 \end{pmatrix} \quad (135)$$

, where l_B is the magnetic length associated to the external field, and we assume that, in a system infinite in the y direction the momentum k_y is conserved. The two signs in Eq. (135) refer to the two valleys in the Brillouin Zone. By squaring the hamiltonian, one obtains the effective Schrödinger equation:

$$\left[-v_F^2 \partial_x^2 + \frac{v_F^2 (x - x_{\pm})^2}{l_B^4} \mp v_F A_y^{strain} \delta(x) \right] \Psi(x) = \epsilon_{k_y}^2 \Psi(x) \quad (136)$$

where $x_- = k_y l_B^2$ and $x_+ = x_- + A_y^{strain}$. For a given value of k_y , the eigenvalue ϵ_{k_y} depends only on v_F and $A_y^{strain} l_B$. The strain induces two effects: i) it shifts the centers of the Landau levels, and ii) a delta function potential appears at the interface. At distances from the interface greater than l_B , the Landau levels are not perturbed, and $\epsilon_{k_y} \rightarrow \pm v_F \sqrt{n}/l_B$, where n is the Landau level index. For $A_y^{strain} l_B \ll 1$ we can use perturbation theory to analyze the shift in the energies of the Landau levels. The leading effect is due to the delta function potential. The maximum change in the energy is:

$$\epsilon_{k_y}^n \approx \pm \frac{v_F \sqrt{n}}{l_B} \left(1 + \pm c_n \frac{A_y l_B}{2n} \right) \quad (137)$$

where c_n is a numerical constant. The Landau levels become dispersive, with a velocity $v^* = \partial \epsilon_{k_y}^n / \partial k_y \approx \pm v_F A_y^{strain} l_B$. The Landau level energy has a maximum, or a minimum, for a value of k_y such that the center is close to the interface. Hence, there are two counter propagating states per Landau level and per valley. These modes have a width $\sim l_B$. Using the Born approximation, it can be shown that the reflection coefficient induced by a single charged impurity is of order e^2/v_F for $A_y^{strain} l_B \sim 1$.

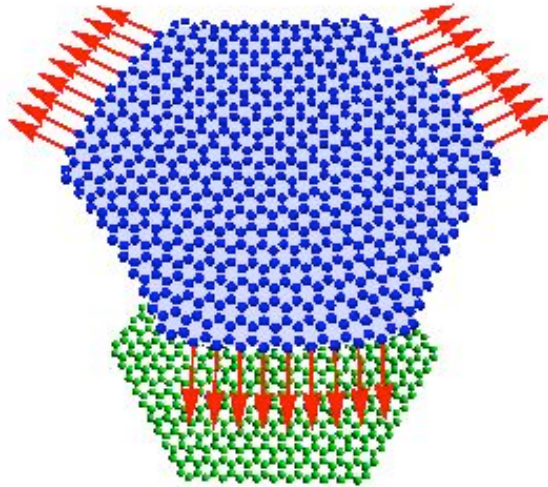


FIG. 18: Sketch of applied strains which lead to an almost constant effective magnetic field inside the sample.

C. Generation of effective magnetic fields. Strain engineering

The previous analysis suggests that strains can generate a wide variety of effective magnetic fields. This has opened the possibility of using “strain engineering” in order to modify the electronic properties of graphene samples [84, 112, 155, 224–233]. Changes in the strain can enhance the chemical activity of graphene, or confine the massless carriers, avoiding the Klein paradox [25]. Experimentally, strains can be induced in graphene flakes by bending the substrate [234–236], and the amount of strain can be measured by Raman spectroscopy. Strains can be due to the difference in expansion coefficients between graphene and the substrate, leading to wrinkles [217]. There is experimental evidence that the electronic properties are modified in strained samples [237].

A particularly interesting possibility is the generation of an effective *constant* magnetic field. The results in the Appendix B show that a strain distribution with trigonal symmetry induces such a field. An experimental setup which leads to an approximate uniform field is shown in Fig. 18, see [227, 232]. Such a situation will change drastically the electronic properties of the system. The electronic spectrum will be split into Landau levels, with counterpropagating chiral modes at the edges. The combination of insulating behavior in the bulk and gapless modes at the edges is reminiscent of a topological insulator [22, 238].

D. Effective electric fields

A time-independent strain gives rise to static gauge fields. Hence, a time-dependent strain will induce effective electric fields [239]. These fields appear in oscillating graphene sheets [180, 240]. As in the static case, the fields acting on different valleys have opposite sign, so that there is no net charge transport and the field is not screened. The time dependence of the scalar potential also induced by the strains [62] also leads to an effective electric field, although with the same sign for the two valleys. This potential can be screened. The effective electric fields induce electronic currents, which dissipate energy. This ohmic damping reduces the quality factor of the oscillator.

The description of the decay of long wavelength phonons into electron-hole pairs by means of an effective electric field acting on the electrons has also been used to understand phonon damping in carbon nanotubes [241] (for a review of the extensive literature on nano electromechanical systems, NEMS, based on carbon nanotubes, see [242]).

In a clean system, the losses due to currents induced by the effective electric fields are equivalent to the phonon lifetime which can be calculated using second order perturbation theory. A formulation using effective fields can easily be extended to diffusive systems, where the electronic wave functions can only be estimated using semiclassical arguments. Standard perturbation theory is adequate for clean, ballistic carbon nanotubes, but a description using a finite mean free path and local conductivities is more appropriate for large graphene samples, as the elastic mean free path is typically much smaller than the dimensions of the sample. It is worth noting that the existence of two counter-propagating valley currents imply that the ohmic dissipation in a graphene resonator is limited, at high temperatures, by valley drag, which, in turn, is dependent on the strength of the electron-electron interaction.

VII. CONCLUSIONS

To summarize, we have presented an overview of the role of gauge fields in graphene and other carbon-based materials. The geometric structure of honeycomb lattice naturally leads, in the continuum limit, to massless Dirac fermions as elementary excitations. The internal degree of freedom which plays the same role as spin in quantum electrodynamics has here a very simple geometric meaning, it is just the sublattice label (pseudospin). Additional internal quantum numbers are the valley label (isospin) and real spin. If we neglect spin-orbit coupling (which is very small in graphene) the latter is split from other degrees of freedom. We distinguish two types of gauge fields: topological, associated to lattice defects, such as disclinations and dislocations, and related to modulations of the hoppings, induced by elastic deformations.

The coupling of the topological fields to the electrons does not depend on the parameters of the material. Topological fields come in two mutually non commuting varieties, depending on whether they mix valleys or not. The gauge fields associated to long wavelength strains do not mix valleys, and their coupling to the electrons depend on the value of the strength of the electron-phonon interaction.

Being exactly a two-dimensional system, graphene shows a thermally induced bending instability which leads to intrinsic ripples (corrugations) even in a free sample. For the case of exfoliated graphene on a substrate, the ripples will arise also due to interaction with the substrate. In both cases, the ripples are sources of a random pseudomagnetic gauge field which modifies the electronic transport in the weak (anti)localization regime, and it also induces essential contributions to the resistivity. The ripples may be one of the main limiting factors restricting mobility of charge carriers in graphene.

Regular gauge fields, or even artificially designed fields can exist in suspended samples, where they can lead to a number of novel features unique to graphene, such as the confinement of electrons, or the formation of localized orbitals similar to the Landau levels which exist in real magnetic fields.

The study of gauge fields in graphene establishes important relations with contemporary mathematical physics. For example, due to the Atiyah-Singer index theorem the gauge fields in both single-layer and bilayer graphene can create states with zero energy, the states being chiral (which means that for a given valley they belong to only one sublattice). The inhomogeneity of pseudomagnetic field created by the ripples should broaden all Landau levels in the quantum Hall regime except the zero-energy one. This prediction of the index theorem can be checked experimentally and seems to be in an agreement with the available data. It is interesting to note that the gauge potentials which arise from lattice deformations have intrinsic meaning, although their effects on the electrons are invariant under gauge transformations, so that different physical deformations can lead to the same electronic structure.

We have not explored here extensions to other systems, such as multilayered graphene, or the topological insulators. The same arguments used to define gauge fields in single layer graphene also apply to multilayered samples. The effect of a given deformation, or gauge field, on the electrons will depend on the number of layers and in the way they are connected. In topological insulators with surface states described by the Dirac equations, gauge fields can also be defined. Because of the different symmetries of these compounds, such fields should arise from perturbations which break time reversal symmetry.

VIII. ACKNOWLEDGMENTS

MAHV thanks A. Cortijo and F. de Juan for many illuminating discussions. FG and MAHV acknowledge support from MEC (Spain) through grant FIS2005-05478-C02-01 and CONSOLIDER CSD2007-00010, and by the Comunidad de Madrid, through CITECNOMIK, CM2006-S-0505-ESP-0337. MK acknowledges support from Stichting voor Fundamenteel Onderzoek der Materie (FOM), the Netherlands.

Appendix A: The Dirac equation in curved space

In general when trying to formulate a mathematical relation defined in a flat space to a curved space, one uses a general covariance principle that amounts to substitute any given magnitude transforming as a tensor in the flat space by the corresponding magnitude transforming as a tensor under general transformations in the curved manifold. This simple substitution is complicated for spinors because there are no spinor representations in the group of general transformations. This makes necessary to introduce an alternative formalism based on tetrads [95, 243]. Instead of the usual metric $g_{\mu\nu}$ we must introduce at each point X described in arbitrary coordinates, a set of locally inertial coordinates ξ_X^a and the vielbein fields $e_\mu^a(x)$, a set of orthonormal vectors labelled by a that fixes the transformation between the local (Latin indices) and the general (Greek indices) coordinates:

$$e_\mu^a(X) \equiv \frac{\partial \xi_X^a(x)}{\partial x^\mu} \Big|_{x=X}. \quad (\text{A1})$$

We can now list the various geometric objects needed to derive the Dirac physics in the curved space: The metric tensor of the curved manifold $g_{\mu\nu}(x)$ is related to the flat, constant metric η_{ab} by the equation

$$g_{\mu\nu}(x) = e_\mu^a(x)e_\nu^b(x)\eta_{ab}; \quad (\text{A2})$$

its determinant, needed to define a scalar density lagrangian is given by

$$\sqrt{-g} = [\det(g_{\mu\nu})]^{1/2} = \det[e_\mu^a(x)]. \quad (\text{A3})$$

The curved space gamma matrices $\gamma^\mu(x)$ satisfying the commutation relations

$$\{\gamma^\mu(x)\gamma^\nu(x)\} = 2g^{\mu\nu}(x), \quad (\text{A4})$$

are related with the constant, flat space matrices γ^a by

$$\gamma^\mu(x) = e_a^\mu(x)\gamma^a. \quad (\text{A5})$$

The most complicated object needed to complete the analysis is the spin connection $\Omega_\mu(x)$ associated to the spinor covariant derivative. This is an important object for the physics since it acts as a gauge field. The construction of the spin connection is done by observing that the derivative of the spinor does not transform as a vector under a coordinate transformation in the flat tangent space. It does if we introduce for the spinors a covariant derivative of the form

$$\mathcal{D}_a = e_a^\mu \left[\frac{\partial}{\partial x^\mu} + \Omega_\mu \right]. \quad (\text{A6})$$

which has a standard transformation under a change of coordinates in both the vector and the spinor indices. To get the structure of the $\Omega_\mu(x)$ matrices it suffices to consider their transformation properties in flat space. For the spin one half representation they take the form

$$\Omega_\mu(x) = \frac{1}{4}\gamma_a\gamma_b e_\lambda^a(x)g^{\lambda\sigma}(x)\nabla_\mu e_\sigma^b(x), \quad (\text{A7})$$

with

$$\nabla_\mu e_\sigma^a = \partial_\mu e_\sigma^a - \Gamma_{\mu\sigma}^\lambda e_\lambda^a \quad (\text{A8})$$

where $\Gamma_{\mu\sigma}^\lambda$ is the usual affine connection which is related to the metric tensor by

$$\Gamma_{\mu\sigma}^\lambda = \frac{1}{2}g^{\nu\lambda} \left\{ \frac{\partial g_{\sigma\nu}}{\partial x^\mu} + \frac{\partial g_{\mu\nu}}{\partial x^\sigma} - \frac{\partial g_{\mu\sigma}}{\partial x^\nu} \right\}. \quad (\text{A9})$$

Finally the Dirac equation is given by

$$i\gamma^\mu(x)[\partial_\mu + \Omega_\mu(x)]\psi(x) = 0. \quad (\text{A10})$$

We will exemplify the formalism by giving the details of the computation of the various geometrical factors for the two main problems described in Section III: the topological defects and the smooth gaussian deformation.

We begin by describing the formalism for a smooth deformation where the curvature is non singular everywhere. We start by embedding a two-dimensional surface with polar symmetry (this is only for simplicity and can be easily extended to any shape) in three-dimensional space (described in cylindrical coordinates). The surface is defined by a function $z(r)$ giving the height with respect to the flat surface $z=0$, and parametrized by the polar coordinates of its projection onto the $z=0$ plane. The metric for this surface is obtained as follows: We compute

$$dz^2 = \left(\frac{dz}{dr}\right)^2 dr^2 \equiv \alpha f(r) dr^2, \quad (\text{A11})$$

and substitute for the line element:

$$ds^2 = dr^2 + r^2 d\theta^2 + dz^2 = (1 + \alpha f(r)) dr^2 + r^2 d\theta^2. \quad (\text{A12})$$

In particular the the gaussian bump shown in Fig. 6 is defined by:

$$z = A \exp(-r^2/b^2), \quad (\text{A13})$$

so that

$$dz^2 = \frac{A^2}{b^4} 4r^2 \exp(-2r^2/b^2) dr^2, \quad (\text{A14})$$

which corresponds to Eq. (A12) with

$$\alpha = (A/b)^2, \quad f(r) = 4(r/b)^2 \exp(-2r^2/b^2).$$

From the line element we can write the metric in a more usual form:

$$g_{\mu\nu} = \begin{pmatrix} -(1 + \alpha f(r)) & 0 \\ 0 & -r^2 \end{pmatrix}, \quad (\text{A15})$$

where we have omitted the time coordinate which is trivial in the case of a static background. The affine connection $\Gamma_{\mu\nu}^\lambda$ which only depends on the metric is for the metric (A15):

$$\Gamma_{rr}^r = \frac{\alpha f'}{2(1 + \alpha f)}, \quad \Gamma_{\theta\theta}^r = -\frac{r}{1 + \alpha f}, \quad \Gamma_{r\theta}^\theta = \frac{1}{r}, \quad (\text{A16})$$

where $f' = df/dr$, and the rest of the elements are zero or related by symmetry.

The geometrical (gaussian) curvature K is

$$K(r) = \frac{\alpha f'(r)}{2r(1 + \alpha f(r))^2}. \quad (\text{A17})$$

The vielbein fields e^a_μ satisfy:

$$g_{\mu\nu} = e^a_\mu e^b_\nu \eta_{ab}, \quad (\text{A18})$$

where η_{ab} is the identity matrix in two dimensions (note that this relation does not fix e^a_μ uniquely). We choose the e^a_μ to be

$$\begin{aligned} e^1_r &= (1 + \alpha f)^{1/2} \cos \theta & e^1_\theta &= -r \sin \theta \\ e^2_r &= (1 + \alpha f)^{1/2} \sin \theta & e^2_\theta &= r \cos \theta; \end{aligned} \quad (\text{A19})$$

that reduce to the flat set when $\alpha = 0$. Now we can compute the spin connection coefficients,

$$\omega_\mu^{ab} = e^a_\nu (\partial_\mu + \Gamma_{\mu\lambda}^\nu) e^{b\lambda}, \quad (\text{A20})$$

which are found to be:

$$\omega_\theta^{12} = 1 - (1 + \alpha f)^{-1/2}, \quad (\text{A21})$$

the rest being zero or related by symmetry (the spin connection ω is antisymmetric in the upper indices [244]).

The spin connection

$$\Omega_\mu = \frac{1}{8}\omega_\mu^{ab} [\gamma_a, \gamma_b], \quad (\text{A22})$$

turns out to be

$$\Omega_r = 0, \quad \Omega_\theta = \frac{1-(1+\alpha f)^{-1/2}}{2}\gamma^1\gamma^2. \quad (\text{A23})$$

In the case of topological defects, for the metric defined by (44):

$$g_{\mu\nu} = \begin{pmatrix} -1 & 0 & 0 \\ 0 & e^{-2\Lambda} & 0 \\ 0 & 0 & e^{-2\Lambda} \end{pmatrix}, \quad (\text{A24})$$

the gamma matrices and the spinor connection in the curved background are immediately found to be

$$\gamma^0(\mathbf{r}) = \gamma^0, \quad \gamma^i(\mathbf{r}) = e^{\Lambda(\mathbf{r})}\gamma^i \quad (i = 1, 2)$$

$$\Omega_1(\mathbf{r}) = -\frac{1}{2}\gamma^1\gamma^2\partial_y\Lambda, \quad \Omega_2(\mathbf{r}) = -\frac{1}{2}\gamma^2\gamma^1\partial_x\Lambda,$$

and the determinant of the metric tensor is

$$\sqrt{-g} = e^{-2\Lambda}.$$

The special feature of the conical defects is that the Riemann curvature tensor is zero everywhere but for the apex of the cone where it has a delta function singularity.

Appendix B: In plane strains and effective fields in radial coordinates

We analyze a circular graphene quantum dot. We first analyze the distribution of stresses. We assume that the dot is free of lattice defects. The stresses are due to forces applied at the boundaries.

The elastic free energy in circular coordinates is:

$$\begin{aligned} \mathcal{F} &= \frac{\lambda}{2} \int 2\pi r dr d\theta \left(\partial_r u_r + \frac{u_r}{r} + \frac{\partial_\theta u_\theta}{r} \right)^2 + \\ &+ \mu \int 2\pi r dr d\theta \left[(\partial_r u_r)^2 + \left(\frac{\partial_\theta u_\theta}{r} + \frac{u_r}{r} \right)^2 + \right. \\ &\left. + \frac{1}{2} \left(\partial_r u_\theta + \frac{\partial_\theta u_r}{r} - \frac{u_\theta}{r} \right)^2 \right] \end{aligned} \quad (\text{B1})$$

where u_r and u_θ are the two components of the displacement vector in circular coordinates. The stress tensor is:

$$\begin{aligned} \sigma_{rr} &= \lambda \left(\partial_r u_r + \frac{\partial_\theta u_\theta}{r} + \frac{u_r}{r} \right) + 2\mu (\partial_r u_r) \\ \sigma_{\theta\theta} &= \lambda \left(\partial_r u_r + \frac{\partial_\theta u_\theta}{r} + \frac{u_r}{r} \right) + 2\mu \left(\frac{\partial_\theta u_\theta}{r} + \frac{u_r}{r} \right) \\ \sigma_{r\theta} &= 2\mu \left(\frac{\partial_\theta u_r}{r} + \partial_r u_\theta - \frac{u_\theta}{r} \right) \end{aligned} \quad (\text{B2})$$

n	a_θ/a_r	$B(r, \theta)$
$-m-1$	$-i$	$4im(m-1)e^{-i(m-2)\theta}r^{m-2}$
$-m+1$	$i \frac{\lambda(m+1)+\mu(m+3)}{\lambda(m-1)+\mu(m-3)}$	$4im(m-1)(m-2) \frac{\lambda+\mu}{\lambda(m-1)+\mu(m-3)} e^{-i(m-4)\theta} r^{m-2}$
$m-1$	$-i \frac{\lambda(m+1)+\mu(m+3)}{\lambda(m-1)+\mu(m-3)}$	$-4im(m-1)(m-2) \frac{\lambda+\mu}{\lambda(m-1)+\mu(m-3)} e^{i(m-4)\theta} r^{m-2}$
$m+1$	i	$-4im(m-1)e^{i(m-2)\theta}r^{m-2}$

TABLE I: Displacements and induced effective magnetic fields for solutions of the equations of elasticity with well defined symmetries under rotations, see Eq. (B4).

The resulting equilibrium equations for u_r and u_θ are:

$$\begin{aligned}
& \lambda \left(-\partial_r^2 u_r - \frac{\partial_r u_r}{r} + \frac{u_r}{r^2} - \frac{\partial_r \partial_\theta u_\theta}{r} + \frac{\partial_\theta u_\theta}{r^2} \right) + \\
& + 2\mu \left(-\frac{\partial_r u_r}{r} - \partial_r^2 u_r + \frac{u_r}{r^2} + \frac{3\partial_\theta u_\theta}{2r^2} - \frac{\partial_\theta^2 u_r}{2r^2} - \frac{\partial_r \partial_\theta u_\theta}{2r} \right) = \\
& = 0 \\
& \lambda \left(-\frac{\partial_r \partial_\theta u_r}{r} - \frac{\partial_\theta u_r}{r^2} - \frac{\partial_\theta^2 u_\theta}{r^2} \right) + \\
& + 2\mu \left(-\frac{3\partial_\theta u_r}{2r^2} - \frac{\partial_\theta^2 u_\theta}{r^2} - \frac{\partial_r u_\theta}{2r} + \frac{u_\theta}{2r^2} - \frac{\partial_r \partial_\theta u_r}{2r} - \frac{\partial_r^2 u_\theta}{2} \right) = \\
& = 0
\end{aligned} \tag{B3}$$

We look for solutions of the type:

$$\begin{aligned}
u_r &= a_r r^m e^{in\theta} \\
u_\theta &= a_\theta r^m e^{in\theta}
\end{aligned} \tag{B4}$$

Inserting these expressions in Eqs. B3, we find:

$$\begin{aligned}
& [\lambda(-m^2+1) + \mu(-2m^2+2+n^2)] a_r + \\
& + (in) [\lambda(-m+1) + \mu(3-m)] a_\theta = 0 \\
& (-in) [\lambda(m+1) + \mu(3+m)] a_r + \\
& [\lambda n^2 + \mu(2n^2 - m^2 + 1)] a_\theta = 0
\end{aligned} \tag{B5}$$

These equations admit solutions for $n = \pm(m \pm 1)$. For $m = 0$ there are only two solutions, with $n = \pm 1$. For $m = 0$, a finite value of a_θ leads to a rotation of the disk, and does not change the physical properties.

The induced gauge field on the Dirac electrons of the graphene layer depends on the relative orientation of the graphene axes. Choosing the direction $\theta = 0$ as one of the lattice axis, the gauge potential can be written as:

$$\begin{aligned}
A_r &= \frac{\beta}{a} \left[\left(\partial_r u_r - \frac{\partial_\theta u_\theta}{r} - \frac{u_r}{r} \right) \cos(3\theta) - \left(\frac{\partial_\theta u_r}{r} + \partial_r u_\theta - \frac{u_\theta}{r} \right) \sin(3\theta) \right] \\
A_\theta &= \frac{\beta}{a} \left[- \left(\partial_r u_r - \frac{\partial_\theta u_\theta}{r} - \frac{u_r}{r} \right) \sin(3\theta) - \left(\frac{\partial_\theta u_r}{r} + \partial_r u_\theta - \frac{u_\theta}{r} \right) \cos(3\theta) \right]
\end{aligned} \tag{B6}$$

where $\beta = \partial \log(t)/\partial \log(a) \approx 2-3$ is the logarithmic derivative of the nearest neighbor hopping t with respect to the nearest neighbor distance, a . The effective magnetic field is:

$$B = \frac{\partial_\theta A_r}{r} - \partial_r A_\theta - \frac{A_\theta}{r} \tag{B7}$$

The effective magnetic fields induced by solutions of equilibrium elasticity of the type described in Eq. (B4) are given in Table[I]. Non trivial solutions which induce a constant field can be obtained by setting $m = 2$ and combining the first and second solutions in Table[I].

[1] L. D. Landau, Phys. Z. Sowjet Union **11**, 26 (1937).

- [2] P. W. Anderson, *Basic Notions of Condensed Matter Physics* (Addison-Wesley, Reading, MA, 1997).
- [3] D. H. Perkins, *Introduction to High Energy Physics* (Cambridge Univ. Press, Cambridge, 2000).
- [4] A. Linde, *Particle Physics and Inflationary Cosmology* (Harwood Acad., Chur, Switzerland, 1990).
- [5] J. C. Collins, *Renormalization* (Cambridge Univ. Press, Cambridge, 1984).
- [6] K. G. Wilson and J. Kogut, *Phys. Rep.* **12**, 75 (1974).
- [7] S. K. Ma, *Modern Theory of Critical Phenomena* (1976).
- [8] K. G. Wilson, *Rev. Mod. Phys.* **47**, 773 (1975).
- [9] A. C. Hewson, *The Kondo Problem to Heavy Fermions* (Cambridge University Press, Cambridge, 1993).
- [10] R. V. Pound and G. A. Rebka, *Phys. Rev. Lett.* **4**, 337 (1960).
- [11] G. E. Volovik, *The Universe in a Helium Droplet* (Clarendon, Oxford, 2003).
- [12] K. S. Novoselov, D. Jiang, F. Schedin, T. J. Booth, V. V. Khotkevich, S. M. Morozov, and A. K. Geim, *PNAS* **102**, 10451 (2005).
- [13] K. S. Novoselov, A. K. Geim, S. V. Morozov, D. Jiang, Y. Zhang, S. V. Dubonos, I. V. Grigorieva, and A. A. Firsov, *Science* **306**, 666 (2004).
- [14] K. S. Novoselov, A. K. Geim, S. V. Morozov, D. Jiang, M. I. Katsnelson, I. V. Grigorieva, S. V. Dubonos, and A. A. Firsov, *Nature* **438**, 197 (2005).
- [15] Y. Zhang, Y.-W. Tan, H. L. Stormer, and P. Kim, *Nature* **438**, 201 (2005).
- [16] A. K. Geim and K. S. Novoselov, *Nature* **6**, 183 (2007).
- [17] M. I. Katsnelson, *Mater. Today* **10**, 20 (2007).
- [18] S. Das Sarma, A. K. Geim, P. Kim, and A. H. MacDonald, *Special Issue of Solid State Commun.* **143**, 1 (2007).
- [19] A. H. Castro Neto, F. Guinea, N. M. R. Peres, K. S. Novoselov, and A. K. Geim, *Rev. Mod. Phys.* **80**, 315 (2008).
- [20] A. K. Geim, *Science* **324**, 1530 (2009).
- [21] G. V. Semenoff, *Phys. Rev. Lett.* **53**, 2449 (1984).
- [22] F. D. M. Haldane, *Phys. Rev. Lett.* **61**, 2015 (1988).
- [23] J. González, F. Guinea, and M. A. H. Vozmediano, *Nucl. Phys. B* **424** [FS], 595 (1994).
- [24] M. I. Katsnelson, *European Physics Journal B* **51**, 1434 (2006).
- [25] M. I. Katsnelson, K. S. Novoselov, and A. K. Geim, *Nature Phys.* **2**, 620 (2006).
- [26] V. V. Cheianov, V. I. Fal'ko, and B. L. Altshuler, *Science* **315**, 1252 (2007).
- [27] M. I. Katsnelson and K. Novoselov, *Solid State Communications* **143**, 3 (2007).
- [28] A. V. Shytov, M. I. Katsnelson, and L. S. Levitov, *Phys. Rev. Lett.* **99**, 246802 (2007).
- [29] C. W. J. Beenakker, *Rev. Mod. Phys.* **80**, 133 (2008).
- [30] O. Klein, *Z. Phys.* **53**, 157 (1929).
- [31] N. Dombey and A. Calogeracos, *Phys. Rep.* **315**, 41 (1999).
- [32] W. Greiner and S. Schramm, *Am. J. Phys. Phys.* **76**, 509 (2008).
- [33] R. V. Gorbachev, A. S. Mayorov, A. K. Savchenko, D. W. Horsell, and F. Guinea, *Nano Lett.* **8**, 1995 (2008).
- [34] N. Stander, B. Huard, and D. Goldhaber-Gordon, *Phys. Rev. Lett.* **102**, 026807 (2009).
- [35] A. F. Young and P. Kim, *Nature Physics* **5**, 222 (2009).
- [36] H. Kleinert, *Gauge fields in condensed matter, vols. 1 and 2* (World Scientific, Singapore, 1989).
- [37] J. F. Sadoc (Editor), *Geometry in Condensed Matter Physics* (World Scientific, Singapore, 1990).
- [38] D. R. Nelson, *Defects and Geometry in Condensed Matter Physics* (Cambridge University Press, Cambridge, 2002).
- [39] G. Toulouse, *Commun. Phys.* **2**, 115 (1977).
- [40] M. O. Katanaev and I. V. Volovich, *Annals of Physics* **216**, 1 (1992).
- [41] S. V. Morozov, K. S. Novoselov, M. I. Katsnelson, F. Schedin, L. A. Ponomarenko, D. Jiang, and A. K. Geim, *Phys. Rev. Lett.* **97**, 016801 (2006).
- [42] A. F. Morpurgo and F. Guinea, *Phys. Rev. Lett.* **97**, 196804 (2006).
- [43] J. C. Meyer, A. K. Geim, M. I. Katsnelson, K. S. Novoselov, T. J. Booth, and S. Roth, *Nature* **446**, 60 (2007).
- [44] J. C. Meyer, A. K. Geim, M. I. Katsnelson, K. S. Novoselov, D. Obergfell, S. Roth, C. Girit, and A. Zettl, *Solid State Communication* **143**, 101 (2007).
- [45] M. Ishigami, J. H. Chen, W. G. Cullen, M. S. Fuhrer, and E. D. Williams, *Nano Letters* **7**, 1643 (2007).
- [46] E. Stolyarova, K. T. Rim, S. Ryu, J. Maultzsch, P. Kim, L. E. Brus, T. F. Heinz, M. S. Hybertsen, and G. W. Flynn, *PNAS* **104**, 9209 (2007).
- [47] A. Fasolino, J. H. Los, and M. I. Katsnelson, *Nature Mater.* **6**, 858 (2007).
- [48] J. González, F. Guinea, and M. A. H. Vozmediano, *Phys. Rev. Lett.* **69**, 172 (1992).
- [49] P. E. Lammert and V. H. Crespi, *Phys. Rev. B* **69**, 035406 (2004).
- [50] A. Cortijo and M. A. H. Vozmediano, *Eur. Phys. Lett.* **77**, 47002 (2007).
- [51] P. R. Wallace, *Phys. Rev.* **71**, 622 (1947).
- [52] J. C. Slonczewski and P. R. Weiss, *Phys. Rev.* **109**, 272 (1958).
- [53] J. L. Mañes, F. Guinea, and M. A. H. Vozmediano, *Phys. Rev. B* **75**, 155424 (2007).
- [54] G. E. Volovik (2006), cond-mat/0601372.
- [55] L. Fu and C. L. Kane, *Phys. Rev. B* **76**, 045302 (2007).
- [56] J. Moore, *Nature Physics* **5**, 378 (2009).
- [57] Y. Xia, D. Qian, D. Hsieh, L. Wray, A. Pal, H. Lin, A. Bansil, D. Grauer, Y. S. Hor, R. J. Cava, et al., *Nature Physics* **5**, 398 (2009).
- [58] J. D. Jackson and L. B. Okun, *Rev. Mod. Phys.* **73**, 663 (2001).

- [59] I. Dzyaloshinskii and G. E. Volovik, *J. de Physique* **39**, 693 (1978).
- [60] I. Dzyaloshinskii and G. E. Volovik, *Ann. Phys.* **125**, 67 (1980).
- [61] E.-A. Kim and A. H. Castro Neto, *Eur. Phys. Lett.* **84**, 57007 (2008).
- [62] H. Suzuura and T. Ando, *Phys. Rev. B* **65**, 235412 (2002).
- [63] J. L. Mañes, *Phys. Rev. B* **76**, 045430 (2007).
- [64] B. T. Kelly, *Physics of Graphite* (Applied Science, London; Englewood, NJ, 1981).
- [65] C. Lee, X. Wei, J. W. Kysar, and J. Hone, *Science* **321**, 5887 (2009).
- [66] K. V. Zakharchenko, M. I. Katsnelson, and A. Fasolino, *Phys. Rev. Lett.* **102**, 046808 (2009).
- [67] D. Kolesnikov and V. A. Osipov, *Eur. Phys. J. B* **49**, 465 (2006).
- [68] C. Furtado, A. M. de M. Carvalho, and C. A. de Lima Ribeiro, *Mod. Phys. Lett. A* **21**, 1393 (2006).
- [69] X. Zhang, K. Jiao, P. Sharma, and B. Yakobson, *Journal of the Mechanics and Physics of Solids* **54**, 2304 (2006).
- [70] Z. Li, P. Dharap, P. Sharma, S. Nagarajaiah, and B. I. Yakobson, *Journal of Applied Physics* **97**, 74303 (2005).
- [71] B. An, S. Fukuyama, K. Yokogawaa, M. Yoshimura, M. Egashira, Y. Korai, and I. Mochida, *Appl. Phys. Lett.* **23** (2001).
- [72] A. Hashimoto, K. Suenaga, A. Gloter, K. Urita, and S. Iijima, *Nature* **430**, 870 (2004).
- [73] E. J. Duplock, M. Scheffler, and P. J. D. Lindan, *Phys. Rev. Lett.* **92** (2004).
- [74] R. Saito, G. Dresselhaus, and M. S. Dresselhaus, *Physical Properties of Carbon Nanotubes* (World Scientific, 1998).
- [75] A. J. Stone and D. J. Wales, *Chem. Phys. Lett.* **128** (1986).
- [76] P. M. Ajayan, V. Ravikumar, and J. C. Charlier, *Phys. Rev. Lett.* **81**, 1437 (1998).
- [77] K. Suenaga, H. Wakabayashi, M. Koshino, Y. Sato, K. Urita, and S. Iijima, *Nature Nanotechnology* **2**, 358 (2007).
- [78] M. B. Nardelli, B. I. Yakobson, and J. Bernholc, *Phys. Rev. B* **57**, R4277 (1998).
- [79] R. Tamura and M. Tsukada, *Phys. Rev. B* **49**, 7697 (1994).
- [80] K. Kobayashi, *Phys. Rev. B* **61**, 8496 (2000).
- [81] J. C. Charlier and G. M. Rignanese, *Phys. Rev. Lett.* **86**, 5970 (2001).
- [82] O. A. Shenderova, B. L. Lawson, D. Areshkin, and D. W. Brenner, *Nanotechnology* **12**, 191 (2001).
- [83] J. K. Pachos, M. Stone, and K. Temme, *Phys. Rev. Lett.* **100**, 156806 (2008).
- [84] S. Ryu, C. Mudry, C. Hou, and C. Chamon, *Phys. Rev. B* **80**, 205319 (2009).
- [85] H. Matsumura and T. Ando, *J. Phys. Soc. of Japan* **67**, 3542 (1998).
- [86] C. L. Kane and E. J. Mele, *Phys. Rev. Lett.* **78**, 1932 (1997).
- [87] E. Mariani, L. I. Glazman, A. Kamenev, and F. von Oppen, *Phys. Rev. B* **76**, 165402 (2007).
- [88] A. Cortijo and M. A. H. Vozmediano, *Nucl. Phys. B* **763**, 293 (2007).
- [89] J. González, F. Guinea, and M. A. H. Vozmediano, *Nucl. Phys. B* **406**, 771 (1993).
- [90] P. E. Lammert and V. H. Crespi, *Phys. Rev. Lett.* **85**, 5190 (2000).
- [91] V. A. Osipov and E. A. Kochetov, *JETP Lett.* **73**, 562 (2001).
- [92] C. Furtado, F. Moraes, and A. M. de M. Carvalho, *Physics Letters A* **372**, 5368 (2008).
- [93] V. A. Osipov and D. Kolesnikov, *Romanian Journal of Physics* **50**, 457 (2005).
- [94] A. Cortijo and M. A. H. Vozmediano, *Eur. Phys. J.* **148**, 83 (2007).
- [95] N. D. Birrell and P. C. W. Davis, *Quantum Fields in Curved Space* (Cambridge University Press, 1982).
- [96] J. González, F. Guinea, and M. A. H. Vozmediano, *Int. J. Mod. Phys. B* **7**, 4331 (1993).
- [97] C. Furtado and F. Moraes, *Phys. Lett. A* **188**, 394 (1994).
- [98] F. Moraes, *Physics Letters A* **214**, 189 (1996).
- [99] Y. Sitenko and N. Vlasii, *Nucl. Phys. B* **787**, 241 (2007).
- [100] T. O. Wehling, A. V. Balatsky, M. I. Katsnelson, A. I. Lichtenstein, K. Scharnberg, and R. Wiesendanger, *Phys. Rev. B* **75**, 125425 (2007).
- [101] F. de Juan, A. Cortijo, and M. A. H. Vozmediano, *Phys. Rev. B* **76**, 165409 (2007).
- [102] A. Vilenkin and E. P. S. Shellard, *Cosmic Strings and Other Topological Defects* (Cambridge University Press, 2000).
- [103] A. Cortijo and M. A. H. Vozmediano, *Phys. Rev. B* **79**, 184205 (2009).
- [104] K. Kondo, *Proceedings of the 2nd Japan national congress for applied mechanics* p. 41 (1952).
- [105] C. Furtado and F. Moraes, *Europhys. Lett.* **45**, 279 (1999).
- [106] F. Moraes, *Brazilian Journal of Physics*, vol. 30, no. 2, June, 2000 **30**, 304 (2000).
- [107] H. S. Seung and D. R. Nelson, *Phys. Rev. A* **38**, 1005 (1988).
- [108] A. Carpio, L. L. Bonilla, F. de Juan, and M. A. H. Vozmediano, *New J. Phys.* **10**, 053021 (2008).
- [109] M. P. López-Sancho, F. de Juan, and M. A. H. Vozmediano, *Phys. Rev. B* **79**, 075413 (2009).
- [110] F. de Juan, A. Cortijo, and M. A. H. Vozmediano, *Nucl. Phys. B* **828**, 625 (2010).
- [111] K. Sasaki, Y. Kawazoe, and R. Saito, *Prog. Theor. Phys.* **113**, 463 (2005).
- [112] S.-M. Choi, S.-H. Jhi, and Y.-W. Son, *Phys. Rev. B* **81**, 081407 (R) (2010).
- [113] S. Ono and K. Sugihara, *J. Phys. Soc. Jap.* **21**, 861 (1966).
- [114] K. Sugihara, *Phys. Rev. B* **28**, 2157 (1983).
- [115] L. Pietronero, S. Strässler, and H. R. Zeller, *Phys. Rev. B* **22**, 904 (1980).
- [116] F. Guinea, *J. Phys. C-Sol. St. Phys.* **14**, 3345 (1981).
- [117] L. M. Woods and G. D. Mahan, *Phys. Rev. B* **61**, 10651 (2000).
- [118] L. Yang, M. P. Anantram, J. Han, and J. Lu, *Phys. Rev. B* **60**, 13874 (1999).
- [119] M. Verissimo-Alves, R. B. Capaz, B. Koiller, E. Artacho, and H. Chacham, *Phys. Rev. Lett.* **86**, 3372 (2001).
- [120] L. D. Landau and E. M. Lifshitz, *Theory of Elasticity* (1970).
- [121] M. M. Fogler, F. Guinea, and M. I. Katsnelson, *Phys. Rev. Lett.* **101**, 226804 (2008).

- [122] F. Guinea, B. Horovitz, and P. L. Doussal, *Phys. Rev. B* **77**, 205421 (2008).
- [123] M. Born and K. Huang, *Dynamical Theory of Crystal Lattices* (Oxford Univ. Press, Oxford, 1998).
- [124] R. E. Peierls, *Helv. Phys. Acta* **7**, 81 (1934).
- [125] R. E. Peierls, *Ann. Inst. H. Poincaré* **5**, 177 (1935).
- [126] L. D. Landau and E. M. Lifshitz (1980).
- [127] N. D. Mermin, *Phys. Rev.* **176** (1968).
- [128] D. Nelson, in *Statistical Mechanics of Membranes and Surfaces*, edited by D. Nelson, T. Piran, and S. Weinberg (World Scientific, Singapore, 1989).
- [129] A. Fasolino, J. H. Los, and M. I. Katsnelson, *Nature Mater.* **6**, 858 (2007).
- [130] W. Helfrich, *Z. Naturforsch.* **28**, 693 (1973).
- [131] S. A. Safran, *Statistical Thermodynamics of Surfaces, Interfaces, and Membranes* (1994).
- [132] L. Peliti and S. Leibler, *Phys. Rev. Lett.* **54**, 690 (1985).
- [133] J. H. Los, M. I. Katsnelson, O. V. Yazyev, K. V. Zakharchenko, and A. Fasolino (2009), arXiv:0903.3847.
- [134] D. R. Nelson and L. Peliti, *J. Physique* **48**, 1085 (1987).
- [135] S. P. Timoshenko and S. Woinowsky-Krieger, *Theory of Plates and Shells* (1959).
- [136] P. L. Doussal and L. Radzihovsky, *Phys. Rev. Lett.* **69**, 1209 (1992).
- [137] X. Xing, R. Mukhopadhyay, T. C. Lubensky, and L. Radzihovsky, *Phys. Rev. E* **68**, 021108 (2003).
- [138] J. J. Binney, N. J. Dowrick, A. J. Fisher, , and M. E. J. Newman, *The Theory of Critical Phenomena* (1992).
- [139] J.-P. Kownacki and D. Mouhanna, *Phys. Rev. E* **79**, 040101(R) (2009).
- [140] J. M. Carlsson and M. Scheffler, *Phys. Rev. Lett.* **96**, 046806 (2006).
- [141] J. H. Los, L. M. Ghiringhelli, E. J. Meijer, and A. Fasolino, *Phys. Rev. B* **72**, 214102 (2005).
- [142] L. M. Ghiringhelli, J. H. Los, E. J. Meijer, A. Fasolino, and D. Frenkel, *Phys. Rev. Lett.* **94**, 145701 (2005).
- [143] M. F. Atiyah and I. M. Singer, *Ann. Math.* **87**, 484 (1968).
- [144] M. F. Atiyah and I. M. Singer, *Proc. Natl. Acad. Sci. USA* **81**, 2597 (1984).
- [145] M. Kaku, *Introduction to Superstrings* (Springer, New York, 1988).
- [146] M. Nakahara, *Geometry, Topology and Physics* (IOP, Bristol, 1990).
- [147] M. I. Katsnelson and M. F. Prokhorova, *Phys. Rev. B* **77**, 205424 (2008).
- [148] K. S. Novoselov, E. McCann, S. V. Morozov, V. I. Fal'ko, M. I. Katsnelson, U. Zeitler, D. Jiang, F. Schedin, and A. K. Geim, *Nature Phys.* **2**, 177 (2006).
- [149] Y. Aharonov and A. Casher, *Phys. Rev. A* **19**, 2461 (1979).
- [150] J. Kailasvuori, *Europhys. Lett.* **87**, 47008 (2009).
- [151] A. J. Giesbers, U. Zeitler, M. I. Katsnelson, L. A. Ponomarenko, T. M. Mohiuddin, and J. C. Maan, *Phys. Rev. Lett.* **99**, 206803 (2007).
- [152] F. Guinea, M. Katsnelson, and M. A. H. Vozmediano, *Phys. Rev. B* **77**, 075422 (2008).
- [153] I. Snyman, *Phys. Rev. B* **80**, 054303 (2009).
- [154] T. O. Wehling, A. V. Balatsky, A. M. Tsvelik, M. I. Katsnelson, and A. I. Lichtenstein, *Europhys. Lett.* **84**, 17003 (2008).
- [155] D. W. Boukhvalov and M. I. Katsnelson, *J. Phys. Chem. C* **113**, 14176 (2009).
- [156] G. Bergman, *Physics Reports* **107**, 1 (1984).
- [157] P. A. Lee and T. V. Ramakrishnan, *Rev. Mod. Phys.* **57**, 287 (1985).
- [158] P. W. Anderson, *Phys. Rev.* **109**, 1492 (1958).
- [159] E. Abrahams, P. W. Anderson, D. C. Licciardello, and T. V. Ramakrishnan, *Phys. Rev. Lett.* **42**, 673 (1979).
- [160] E. McCann, K. Kechedzhi, V. I. Fal'ko, H. Suzuura, T. Ando, and B. L. Altshuler, *Phys. Rev. Lett.* **97**, 146805 (2006).
- [161] F. V. Tikhonenko, D. W. Horsell, R. V. Gorbachev, and A. K. Savchenko, *Phys. Rev. Lett.* **100**, 056802 (2008).
- [162] R. V. Gorbachev, F. V. Tikhonenko, A. S. Mayorov, D. W. Horsell, and A. K. Savchenko, *Phys. Rev. Lett.* **98**, 176805 (2007).
- [163] A. Altland and B. Simons, *Condensed Matter Field Theory* (Cambridge University Press, 2006).
- [164] E. Fradkin, *Phys. Rev. B* **33**, 3257 (1986).
- [165] E. Fradkin, *Phys. Rev. B* **33**, 3263 (1986).
- [166] A. W. W. Ludwig, M. P. A. Fisher, R. Shankar, and G. Grinstein, *Phys. Rev. B* **50**, 7526 (1994).
- [167] J. Ye and S. Sachdev, *Phys. Rev. Lett.* **80**, 5409 (1998).
- [168] C. de C. Chamon, C. Mudry, and X.-G. Wen, *Phys. Rev. Lett.* **77**, 4194 (1996).
- [169] P. M. Ostrovsky, I. V. Gornyi, and A. D. Mirlin, *Phys. Rev. B* **74**, 235443 (2006).
- [170] I. L. Aleiner and K. B. Efetov, *Phys. Rev. Lett.* **97**, 236801 (2006).
- [171] E. McCann, K. Kechedzhi, V. Fal'ko, H. Suzuura, T. Ando, and B. Altshuler, *Phys. Rev. Lett.* **97**, 146805 (2006).
- [172] J. Ye, *Phys. Rev. B* **60**, 8290 (1999).
- [173] J. González, F. Guinea, and M. A. H. Vozmediano, *Phys. Rev. B* **63**, 134421 (2001).
- [174] T. Stauber, F. Guinea, and M. A. H. Vozmediano, *Phys. Rev. B* **71**, 041406(R) (2005).
- [175] O. Vafek and M. J. Case, *Phys. Rev. B* **77**, 033410 (2008).
- [176] M. S. Foster and I. L. Aleiner, *Phys. Rev. B* **77**, 195413 (2008).
- [177] K. Nomura and A. H. MacDonald, *Phys. Rev. Lett.* **96**, 256602 (2006).
- [178] D. V. Khveshchenko, *Phys Rev B* **75**, 241406(R) (2007).
- [179] J. González, F. Guinea, and M. A. H. Vozmediano, *Phys. Rev. B* **59**, R2474 (1999).
- [180] K. I. Bolotin, K. J. Sikes, Z. Jiang, G. Fudenberg, J. Hone, P. Kim, and H. L. Stormer, *Solid State Communications* **146**, 351 (2008).

- [181] X. Du, I. Skachko, A. Barker, and E. Y. Andrei, *Nature Nanotechnology* **3**, 491 (2008).
- [182] M. I. Katsnelson, *Phys. Rev. B* **74**, 201401(R) (2006).
- [183] M. Auslender and M. I. Katsnelson, *Phys. Rev. B* **76**, 235425 (2007).
- [184] J. M. Ziman, *Electrons and Phonons - the Theory of Transport Phenomena in Solids* (2001).
- [185] N. H. Schon and T. Ando, *J. Phys. Soc. Japan* **67**, 1209 (1998).
- [186] M. Hentschel and F. Guinea, *Phys. Rev. B* **76**, 115407 (2007).
- [187] D. S. Novikov, *Phys. Rev. B* **76**, 245435 (2007).
- [188] J. Cserti, A. Palyi, and C. Peterfalvi, *Phys. Rev. Lett.* **99**, 246801 (2007).
- [189] A. V. Shytov, M. I. Katsnelson, and L. S. Levitov, *Phys. Rev. Lett.* **99**, 236801 (2007).
- [190] F. Guinea, *Journ. Low Temp. Phys.* **153**, 359 (2008).
- [191] M. Born and E. Wolf, *Principles of Optics* (1980).
- [192] L. D. Landau and E. M. Lifshitz, *Quantum Mechanics* (1977).
- [193] T. Stauber, N. M. R. Peres, and F. Guinea, *Phys. Rev. B* **76**, 205423 (2007).
- [194] M. I. Katsnelson and A. K. Geim, *Philos. Trans. R. Soc. (London)* **Ser. A 366**, 195 (2008).
- [195] V. M. Pereira, J. Nilsson, and A. H. Castro Neto, *Phys. Rev. Lett.* **99**, 166802 (2007).
- [196] T. Ando, *J. Phys. Soc. Japan* **75**, 074716 (2006).
- [197] S. Adam, E. H. Hwang, V. M. Galitski, and S. D. Sarma, *Proc. Natl. Acad. Sci. USA* **104**, 18392 (2007).
- [198] C. Jang, S. Adam, J.-H. Chen, E. D. Williams, S. D. Sarma, , and M. S. Fuhrer, *Phys. Rev. Lett.* **101**, 146805 (2008).
- [199] F. Schedin, A. Geim, S. Morozov, E. Hill, P. Blake, M. Katsnelson, and K. Novoselov, *Nature Materials* **6**, 652 (2007).
- [200] L. A. Ponomarenko, R. Yang, T. M. Mohiuddin, M. I. Katsnelson, K. S. Novoselov, S. V. Morozov, A. A. Zhukov, F. Schedin, E. W. Hill, and A. K. Geim, *Phys. Rev. Lett.* **102**, 206603 (2009).
- [201] M. I. Katsnelson, F. Guinea, and A. K. Geim, *Phys. Rev. B* **79**, 195426 (2009).
- [202] T. O. Wehling, M. I. Katsnelson, and A. I. Lichtenstein, *Phys. Rev. B* **80**, 085428 (2009).
- [203] T. O. Wehling, M. I. Katsnelson, and A. I. Lichtenstein, *Chem. Phys. Lett.* **476**, 125 (2009).
- [204] J. H. Chen, W. G. Cullen, C. Jang, M. S. Fuhrer, and E. D. Williams, *Phys. Rev. Lett.* **102**, 236805 (2009).
- [205] R. Kubo, *J. Phys. Soc. Japan* **12**, 570 (1957).
- [206] H. Nakano, *Prog. Theor. Phys.* **17**, 145 (1957).
- [207] H. Mori, *Prog. Theor. Phys.* **34**, 399 (1965).
- [208] V. Y. Irkhin and M. I. Katsnelson, *Eur. Phys. J. B* **30**, 481 (2002).
- [209] S. V. Morozov, K. S. Novoselov, M. I. Katsnelson, F. Schedin, D. C. Elias, J. A. Jaszczak, and A. K. Geim, *Phys. Rev. Lett.* **100**, 016602 (2008).
- [210] V. Geringer, M. Liebmann, T. Echtermeyer, Runte, M. Schmidt, R. Rckamp, M. C. Lemme, and M. Morgenstern, *Phys. Rev. Lett.* **102**, 076102 (2009).
- [211] E. Mariani and F. von Oppen, *Phys. Rev. Lett.* **100**, 249901 (2008).
- [212] K. I. Bolotin, K. J. Sikes, Z. Jiang, G. Fudenberg, J. Hone, P. Kim, and H. L. Stormer, *Sol. St. Commun.* **156**, 351 (2008).
- [213] V. Geringer, M. Liebmann, T. Echtermeyer, S. Runte, R. Rückamp, M. Lemme, and M. Morgenstern, *Phys. Rev. Lett.* **102**, 076102 (2009).
- [214] J. S. Bunch, S. S. Verbridge, J. S. Alden, A. M. van der Zande, J. M. Parpia, H. G. Craighead, and P. L. McEuen, *Nano Lett.* **8**, 2458 (2008).
- [215] K. I. Bolotin, K. J. Sikes, J. Hone, H. L. Stormer, and P. Kim, *Phys. Rev. Lett.* **101**, 096802 (2008).
- [216] S. Berciaud, S. Ryu, L. E. Brus, and T. F. Heinz, *Nano Lett.* **9**, 346 (2009).
- [217] W. Bao, F. Miao, Z. Chen, H. Zhang, W. Jang, C. Dames, and C. N. Lau, *Nature Nanotechnology* **4**, 562 (2009).
- [218] J. Velasco Jr., G. Liu, W. Bao, and C. N. Lau, *New J. Phys.* **11**, 095008 (2009).
- [219] C. Chen, S. Rosenblatt, K. I. Bolotin, W. Kalb, P. Kim, I. Kymissis, H. L. Stormer, T. F. Heinz, and J. Hone (2009), arXiv:0907.3721.
- [220] A. Kormányos, P. Rakytka, L. Oroszlány, and J. Cserti, *Phys. Rev. B* **78**, 045430 (2008).
- [221] M. R. Masir, P. Vasilopoulos, A. Matulis, and F. Peeters, *Phys. Rev. Lett.* **77**, 235443 (2008).
- [222] M. R. Masir, P. Vasilopoulos, and F. Peeters, *New J. Phys.* **11**, 095009 (2009).
- [223] G. León, E. Prada, P. San-José, M. M. Fogler, and F. Guinea (2009), arXiv:0906.5267.
- [224] V. M. Pereira and A. H. Castro Neto, *Phys. Rev. Lett.* **103**, 046801 (2009).
- [225] P. L. de Andrés and J. A. Vergés, *Appl. Phys. Lett.* **93**, 171915 (2008).
- [226] V. M. Pereira, A. H. C. Neto, and N. M. Peres, *Phys. Rev. B* **80**, 045401 (2009).
- [227] F. Guinea, M. I. Katsnelson, and A. K. Geim, *Nature Phys.* **6**, 30 (2010).
- [228] M. Farjam and H. Rafii-Tabar (2009), arXiv:0909.5052.
- [229] J. Viana-Gomes, V. M. Pereira, and N. M. Peres (2009), arXiv:0909.5052.
- [230] M. Mohr, K. Papagelis, J. Maultzsch, and C. Thomsen (2009), arXiv:0908.0895.
- [231] T. G. Rappoport, B. Uchoa, and A. H. Castro Neto (2009), arXiv:0906.2194.
- [232] F. Guinea, A. K. Geim, M. I. Katsnelson, and K. S. Novoselov, *Phys. Rev. B* **81**, 035408 (2010).
- [233] S.-M. Choi, S.-H. Jhi, and Y.-W. Son (20010), arXiv:1002.4685.
- [234] T. M. Mohiuddin, A. Lombardo, R. R. Nair, A. Bonetti, G. Savini, R. Jalil, N. Bonini, D. M. Basko, C. Galiotis, N. Marzari, K. S. Novoselov, A. K. Geim, and A. C. Ferrari, *Phys. Rev. B* **79**, 205433 (2009).
- [235] M. Huang, H. Yan, C. Chen, D. Song, T. F. Heinz, and J. Hone, *Proc. Nat. Ac. Sci. (USA)* **106**, 7304 (2009).
- [236] G. Tsoukleri, J. Parthenios, K. Papagelis, R. Jalil, A. C. Ferrari, A. K. Geim, K. S. Novoselov, and C. Galiotis, *Small* (2009), DOI: 10.1002/sml.200900802.

- [237] M. L. Teague, A. P. Lai, J. Velasco, C. R. Hughes, A. D. Beyer, M. W. Bockrath, C. N. Lau, and N.-C. Yeh, *Nano Lett.* **9**, 2542 (2009).
- [238] C. L. Kane and E. J. Mele, *Phys. Rev. Lett* **95**, 226801 (2005).
- [239] F. von Oppen, F. Guinea, and E. Mariani, *Phys. Rev. B* **80**, 075420 (2009).
- [240] D. Garcia-Sanchez, A. M. van der Zande, A. S. Paulo, B. Lassagne, P. L. McEuen, and A. Bachtold, *Nano Lett.* **8**, 1399 (2008).
- [241] K. Sasaki, R. Saito, G. Dresselhaus, M. S. Dresselhaus, H. Farhat, and J. Kong, *Phys. Rev. B* **78**, 235405 (2008).
- [242] A. K. Hüttel, M. Poot, B. Witkamp, and H. S. J. van der Zant, *New Journ. Phys.* **10**, 095003 (2008).
- [243] S. Weinberg, *The quantum theory of fields* (Cambridge University Press, 1996).
- [244] S. Weinberg, *Gravitation and cosmology: principles and applications to the general theory of relativity* (Wiley and Sons, 1972).